

1 **CORRELATION BETWEEN TECTONIC STRESS REGIMES AND METHANE SEEPAGE ON THE**
2 **WEST-SVALBARD MARGIN**

3
4 A. Plaza-Faverola¹ and M. Keiding²

5 ¹ CAGE-Centre for Arctic Gas Hydrate, Environment, and Climate; Department of Geosciences, UiT The Arctic
6 University of Norway, N-9037 Tromsø, Norway

7 ² Geological Survey of Norway (NGU), P.O. Box 6315 Torgarden, 7491 Trondheim, Norway

8 *Correspondence to:* Andreia Plaza-Faverola (Andreia.a.faverola@uit.no)

9 **Abstract.** Methane seepage occurs across the west-Svalbard margin at water depths ranging from < 300 m,
10 landward from the shelf break, to > 1000 m in regions just a few kilometres away from the mid-ocean ridges in
11 the Fram Strait. The mechanisms controlling seepage remain elusive. The Vestnesa sedimentary ridge, located on
12 oceanic crust at 1000-1700 m water depth, hosts a perennial gas hydrate and associated free gas system. The
13 restricted occurrence of acoustic flares to the eastern segment of the sedimentary ridge, despite the presence of
14 pockmarks along the entire ridge, indicates a spatial variation in seepage activity. This variation coincides with a
15 change in the faulting pattern as well as in the characteristics of fluid flow features. Due to the position of the
16 Vestnesa ridge with respect to the Molloy and Knipovich mid-ocean ridges, it has been suggested that seepage
17 along the ridge has a tectonic control. We modelled the tectonic stress regime due to oblique spreading along the
18 Molloy and Knipovich ridges to investigate whether spatial variations in the tectonic regime along the Vestnesa
19 Ridge are plausible. The model predicts a zone of tensile stress that extends northward from the Knipovich Ridge
20 and encompasses the zone of acoustic flares on the eastern Vestnesa Ridge. In this zone the orientation of the
21 maximum principal stress is parallel to pre-existing faults. The model predicts a strike-slip stress regime in
22 regions with pockmarks where acoustic flares have not been documented. If a certain degree of coupling is
23 assumed between deep crustal and near-surface deformation, it is possible that ridge push forces have influenced
24 seepage activity in the region by interacting with the pore-pressure regime at the base of the gas hydrate stability
25 zone. More abundant seepage on the eastern Vestnesa Ridge at present may be facilitated by dilation of faults and
26 fractures favourably oriented with respect to the stress field. A modified state of stress in the past, for instance
27 due to more significant glacial stress, may have explained a vigorous seepage activity along the entire Vestnesa
28 Ridge. The contribution of other mechanisms to the state of stress (i.e., sedimentary loading and lithospheric
29 flexure) remain to be investigated. Our study provides a first order assessment of how tectonic stresses may be
30 influencing the kinematics of near-surface faults and associated seepage activity offshore the west-Svalbard
31 margin.

32

33

34 **1. Introduction**

35 Hundreds of gigatonnes of carbon are stored as gas hydrates and shallow gas reservoirs in continental margins
36 (e.g., Hunter et al., 2013). The release of these carbons over geological time, a phenomenon known as methane
37 seepage, is an important contribution to the global carbon cycle. Understanding and quantifying seepage has
38 important implications for ocean acidification, deep-sea ecology and global climate. Periods of massive methane
39 release from gas hydrate systems (e.g., Dickens, 2011) or from large volcanic basins like that in the mid-
40 Norwegian margin (e.g., Svensen et al., 2004) have been linked to global warming events such as the Palaeocene-
41 Eocene thermal maximum. In addition, methane seepage and near-seafloor gas migration have implications for
42 geohazards, since pore-fluid pressure destabilization is one factor associated with the triggering of submarine
43 land-slides (e.g., DeVore and Sawyer, 2016; Urlaub et al., 2015). It is well known that seepage at continental
44 margins has been occurring episodically for millions of years (e.g., Judd and Hovland, 2009), but there is a poor
45 understanding of what forces it.

46

47 Present day seepage is identified as acoustic flares in the water column commonly originating at seafloor
48 depressions (e.g., Chand et al., 2012; Salomatin and Yusupov, 2011; Skarke et al., 2014; Smith et al.,
49 2014; Westbrook et al., 2009), while authigenic carbonate mounds are used as indicators of longer-term seepage
50 activity (e.g., Judd and Hovland, 2009). Seepage at the theoretical upstream termination of the gas hydrate
51 stability zone (GHSZ) (i.e., coinciding with the shelf edge) at different continental margins, has been explained
52 by temperature driven gas-hydrate dissociation (e.g., Skarke et al., 2014; Westbrook et al., 2009). On formerly
53 glaciated regions off Svalbard and the Barents Sea, active seepage has been explained by gas hydrate dissociation
54 either due to pressure changes resulting from the retreat of the ice-sheet (e.g., Portnov et al., 2016; Andreassen et
55 al., 2017) or to post-glacial uplift (Wallmann et al., 2018).

56

57 Across the west-Svalbard margin, active seepage extends beyond the shelf break and the region formerly covered
58 by ice. As a matter of fact, active seepage sites have been identified from inside Isfjorden (Roy et al., 2014) to
59 water depths of ~1200 m (Smith et al., 2014) where the Vestnesa Ridge hosts a perennially stable gas hydrate
60 system > 50 km seaward from the ice-sheet grounding line. The Vestnesa Ridge is a NW-SE oriented contourite
61 deposit located between the northward termination of the Knipovich Ridge and the eastern flank of the Molloy
62 spreading ridge in the Fram Strait (Fig. 1). Seafloor pockmarks along the Vestnesa Ridge, first documented by

63 Vogt et al., (1994), exist along the entire ridge. However, acoustic flares have been observed to originate
64 exclusively at large pockmarks located on the eastern part of the sedimentary ridge (Fig. 2, 3). A clear increase in
65 seepage activity towards the easternmost part of the ridge is thus evident from multiple year's water-column
66 acoustic surveys (Petersen et al., 2010;Bünz et al., 2012;Plaza-Faverola et al., 2017;Smith et al., 2014). In this
67 paper, we use the terminology “active” and “inactive” to differentiate between sites with and without documented
68 acoustic flares. Even though methane advection and methanogenesis are likely to be active processes along the
69 entire Vestnesa Ridge, the presence of inactive pockmarks adjacent to a zone of active seepage, raises the
70 question what controls temporal and spatial variations in seepage activity along the ridge?

71

72 Plaza-Faverola et al., (2015) documented seismic differences in the orientation and type of faulting along the
73 ridge and showed a link between the distribution of gas chimneys and faults. They hypothesised that seepage
74 activity may be explained by spatial variation in tectonic stress field across the margin (Plaza-Faverola et al.,
75 2015). However, the state of stress across Arctic passive margins has not been investigated. The total state of
76 stress at formerly glaciated continental margins can be the result of diverse factors including bathymetry and
77 subsurface density contrasts, subsidence due to glacial or sedimentary loading and lithospheric cooling, in
78 addition to ridge-push forces (Fejerskov and Lindholm, 2000;Lindholm et al., 2000;Olesen et al., 2013;Stein et
79 al., 1989;Grunnaleite et al., 2009).

80

81 The interaction between the above mentioned factors renders modelling of the total state of stress a complex
82 problem that has not yet been tackled. In this study, we focus exclusively on the potential contribution of oblique
83 spreading at the Molloy and the Knipovich ridges to the total state of stress along the Vestnesa Ridge and do a
84 qualitative analysis of how stress generated by mid-ocean ridge spreading may influence near-surface faulting
85 and associated seepage activity. The study of the effect of ridge push forces on near-surface deformation across
86 the west-Svalbard margin contributes to the current debate about neo-tectonism and stress field variations across
87 passive margins (Olesen et al., 2013;Salomon et al., 2015). It also has implications for understanding the
88 mechanisms that control seepage at continental margins globally. Splay-faults are found to drive fluid migration
89 at subduction margins and to sustain shallow gas accumulations and seepage (e.g., Plaza-Faverola et al.,
90 2016;Minshull and White, 1989;Moore and Vrolijk, 1992;Crutchley et al., 2013), and the relationship between
91 fault kinematics and fluid migration has been documented specially at accretionary margins where earthquake-
92 induced seafloor seepage has been observed (e.g., Geersen et al., 2016). So far, the information about the present
93 day stress regime in the Fram Strait has been limited to large scale lithospheric density models (Schiffer et al.,

94 2018) and a number of stress vectors from earthquake focal mechanisms along the mid-Atlantic plate boundary
95 (Heidbach et al., 2016). Our study provides a first order assessment of how stresses from slow spreading mid-
96 ocean ridges may be influencing the kinematics of near-surface faults and associated seepage activity across an
97 Arctic passive margin.

98

99 **2. Structural and stratigraphic setting**

100 In the Fram Strait, sedimentary basins are within tens of kilometres from ultra-slow spreading Arctic mid-ocean
101 ridges (Fig. 1). The opening of the Fram Strait was initiated 33 Ma ago and evolved as a result of slow spreading
102 of the Molloy and Knipovich Ridges (Engen et al., 2008). An important transpressional event deformed the
103 sedimentary sequences off western Svalbard, resulting in folds and thrustbelts, during the Paleocene-Eocene
104 dextral movement of Spitsbergen with respect to Greenland. Transpression stopped in the early Oligocene when
105 the tectonic regime became dominated by extension (Myhre and Eldholm, 1988). The circulation of deep water
106 masses through the Fram Strait started during the Miocene, ca. 17-10 Ma ago (Jakobsson et al., 2007; Ehlers and
107 Jokat, 2009), and established the environmental conditions for the evolution of bottom current-driven
108 sedimentary drifts (Eiken and Hinz, 1993; Johnson et al., 2015). It has been suggested that the opening of the
109 northern Norwegian–Greenland Sea was initiated by the northward propagation of the Knipovich ridge into the
110 ancient Spitsbergen Shear Zone (Crane et al., 1991).

111

112 The continental crust beneath the western coast of Svalbard thins towards the Hornsund Fault zone indicating
113 extension following the opening of the Greenland Sea (Faleide et al., 1991). Late Miocene and Pliocene
114 sedimentation, driven by bottom currents, resulted in the formation of the ca. 100 km long Vestnesa Ridge
115 between the shelf break off west-Svalbard and oceanic crust highs at the eastern flank of the Molloy mid-ocean
116 ridge (Eiken and Hinz, 1993; Vogt et al., 1994). The sedimentary ridge is oriented parallel to the Molloy
117 Transform Fault and its crest experiences a change in morphology from narrow on the eastern segment to broader
118 on the western Vestnesa Ridge segment (Fig. 2). The exact location of the continental-ocean transition remains
119 uncertain (Eldholm et al., 1987) but it is inferred to be nearby the transition from the eastern to the western
120 segments (Engen et al., 2008).

121

122 The total sedimentary thickness along the Vestnesa Ridge remains unconstrained. Based on one available
123 regional seismic profile it can be inferred that the ridge is > 5 km thick in places (Eiken and Hinz, 1993). It has
124 been divided into three main stratigraphic units (Eiken and Hinz, 1993; Hustoft, 2009): the deepest sequence,

125 YP1, consists of synrift and post-rift sediments deposited directly on oceanic crust; YP2 consists of contourites;
126 and YP3, corresponding to the onset of Pleistocene glaciations (ca. 2.7 Ma ago) (Mattingsdal et al., 2014), is
127 dominated by glaciomarine contourites and a mix with turbidites in regions close to the shelf break. The effect of
128 ice-sheet dynamics on the west-Svalbard margin (Patton et al., 2016;Knies et al., 2009) has influenced the
129 stratigraphy, and most likely the morphology, of the Vestnesa Ridge and adjacent sedimentary basins. In this
130 Arctic region, glaciations are believed to have started even earlier than 5 Ma ago. The local intensification of
131 glaciations is inferred to have started ca. 2.7 Ma ago (e.g., Faleide et al., 1996;Mattingsdal et al., 2014). Strong
132 climatic fluctuations characterized by intercalating colder, intense glaciations with warmer and longer
133 interglacials, dominated the last ca. 1 Ma. (e.g., Jansen et al., 1990;Jansen and Sjøholm, 1991).

134

135 **3. Seismic data**

136 The description of faults and fluid flow related features along the Vestnesa Ridge is documented by several
137 authors (Bünz et al., 2012;Hustoft, 2009;Petersen et al., 2010;Plaza-Faverola et al., 2015;Plaza-Faverola et al.,
138 2017). Two-3D high resolution seismic data sets acquired on the western and the eastern Vestnesa Ridge
139 respectively (Fig. 2), and one 2D seismic line acquired along the entire Vestnesa Ridge extent have been
140 particularly useful in the description of the structures along the ridge (Fig. 2). These data have been previously
141 used for the investigation of the bottom simulating reflection dynamics (i.e., the seismic indicator of the base of
142 the gas hydrate stability zone) (Plaza-Faverola et al., 2017) and documentation of gas chimneys and faults in the
143 region (Petersen et al., 2010;Plaza-Faverola et al., 2015;Bünz et al., 2012). The 3D seismic data were acquired on
144 board R/V Helmer Hanssen using the high resolution P-Cable system (Planke et al., 2009). The 2D lines were
145 also collected connecting 4 streamers from the P-Cable system for 2D acquisition. Final lateral resolution of the
146 3D data sets is given by a bin size of 6.25x6.25 m² and the vertical resolution is > 3 m with a dominant frequency
147 of 130 Hz. Details about acquisition and processing can be found in Petersen et al., 2010 and Plaza-Faverola et
148 al., 2015. For the 2D survey the dominant frequency was ~80 Hz resulting in a vertical resolution > 4.5 m
149 (assumed as $\lambda/4$ with an acoustic velocity in water of 1469 m/s given by CTD data; Plaza-Faverola et al., 2017).

150

151 **4. The modelling approach**

152 The modelling carried out in this study deals exclusively with tectonic stress due to ridge push. We use the
153 approach by Keiding et al. (2009) based on the analytical solutions derived by Okada (1985), to model the plate
154 motion and tectonic stress field due to spreading along the Molloy and Knipovich Ridges.

155

156 The Okada model and our derivation of the stress field from it is described in more detail in appendix A. The
157 Molloy and Knipovich Ridges are modelled as rectangular planes with opening and transform motion in a flat
158 Earth model with elastic, homogeneous, isotropic rheology (Fig. A1 in appendix). Each rectangular plane is
159 defined by ten model parameters used to approximate the location, geometry and deformation of the spreading
160 ridges (Okada, 1985; see supplement Table 1). The locations of the two spreading ridges were constrained from
161 bathymetry maps (Fig. 1). The two spreading ridges are assumed to have continuous, symmetric deformation
162 below the brittle-ductile transition, with a half spreading rate of 7 mm/yr and a spreading direction of N125°E,
163 according to recent plate motion models (DeMets et al., 2010). Because the spreading direction is not
164 perpendicular to the trends of the spreading ridges, this results in both opening and right-lateral motion; that is,
165 oblique spreading on the Molloy and Knipovich Ridges. The Molloy Transform Fault, which connects the two
166 spreading ridges, trends N133°E, thus a spreading direction of N125°E implies extension across the transform
167 zone. We use a depth of 10 km for the brittle-ductile transition and 900 km for the lower boundary of the
168 deforming planes, to avoid boundary effects. For the elastic rheology, we assume typical crustal values of
169 Poisson's ratio = 0.25 and shear modulus = 30 GPa (Turcotte and Schubert, 2002). We perform sensitivity tests
170 for realistic variations in 1) model geometry, 2) spreading direction, 3) depth of the brittle-ductile transition, and
171 4) Poisson's ratio (Supplementary material). Variations in shear modulus, e.g. reflecting differences in elastic
172 parameters of crust and sediments, would not influence the results, because we do not consider the magnitude of
173 the stresses.

174

175 Asymmetric spreading has been postulated for the Knipovich Ridge based on heat flow data (Crane et al., 1991),
176 and for other ultraslow spreading ridges based on magnetic data (e.g., Gaina et al., 2015). However, the evidence
177 for asymmetry along the Knipovich Ridge remains inconclusive and debatable in terms, for example, of the
178 relative speeds suggested for the North American (faster) and the Eurasian (slower) plates (Crane et al.,
179 1991; Morgan, 1981; Vogt et al., 1994). This reflects that the currently available magnetic data from the west-
180 Svalbard margin is not of a quality that allows an assessment of possible asymmetry of the spreading in the Fram
181 Strait (Nasuti and Olesen, 2014). Symmetry is thus conveniently assumed for the purpose of the present study.

182

183 We focus on the stress field in the upper part of the crust (where the GHSZ is) and characterise the stress regime
184 based on the relationship between the horizontal and vertical stresses. We refer to the stresses as σ_v (vertical
185 stress), σ_H (maximum horizontal stress) and σ_h (minimum horizontal stress), where compressive stress is positive
186 (Zoback and Zoback, 2002). A tensile stress regime ($\sigma_v > \sigma_H > \sigma_h$) favours the opening of steep faults that can

187 provide pathways for fluids. Favourable orientation of stresses with respect to existing faults and/or pore fluid
188 pressures increasing beyond hydrostatic pressures are additional conditions for leading to opening for fluids
189 under strike-slip ($\sigma_H > \sigma_v > \sigma_h$) and compressive ($\sigma_H > \sigma_h > \sigma_v$) regimes (e.g., Grauls and Baleix, 1994).

190

191 **5. Results**

192 **5.1 Predicted type and orientation of stress fields due to oblique spreading at the Molloy and the Knipovich** 193 **ridges**

194 The model predicts zones of tensile stress near the spreading ridges, and strike-slip at larger distances from the
195 ridges. An unexpected pattern of tensile stress arises from the northward termination and the southward
196 termination of the Knipovich and Molloy ridges respectively (Fig. 3). The zone of tensile stress that extends
197 northward from the Knipovich Ridge, encompasses the eastern part of the Vestnesa Ridge. The western Vestnesa
198 Ridge, on the other hand, lies entirely in a zone of strike-slip stress (Fig. 3). The sensitivity tests show that the
199 tensile stress zone is a robust feature of the model, that is, variations in the parameters result in a change of the
200 extent and shape of the tensile zone but the zone remains in place (Supplementary material). It appears that the
201 tensile zone is a result of the interference of the stress from the two spreading ridges. To illustrate this, we ran the
202 model for the Molloy Ridge and the Knipovich Ridge independently. In the model with Knipovich Ridge alone, a
203 large tensile zone extends northeast from the ridge's northern end, covering only the easternmost corner of
204 Vestnesa Ridge (Fig. 4). Under the influence of the strike-slip field from the Molloy Ridge, this zone is deflected
205 and split into two lobes, of which one extends to the eastern Vestnesa Ridge segment.

206

207 To investigate the geometric relationship between the predicted stress field and mapped faults, we calculated the
208 orientations of maximum compressive horizontal stress (Lund and Townend, 2007). The maximum horizontal
209 stresses (σ_H) approximately align with the spreading axes within the tensile regime and are perpendicular to the
210 axes within the strike-slip regime (Fig. 3). Spreading along the Molloy ridge causes NW-SE orientation of the
211 maximum compressive stress along most of the Vestnesa Ridge, except for the eastern segment where the
212 influence of the Knipovich Ridge results in a rotation of the stress towards E-W (Fig. 3).

213

214 The simplifying assumptions involved in our model imply that the calculated stresses in the upper crust are
215 unconstrained to a certain degree. However, the predicted stress directions are in general agreement with other
216 models of plate tectonic forces (e.g., Gölke and Coblenz, 1996; Naliboff et al., 2012). In addition, Árnadóttir et
217 al. (2009) demonstrated that the deformation field from the complex plate boundary in Iceland could be modelled

218 using Okada's models. More importantly, a comparison of the predicted strike-slip and tensile stress fields from
219 plate spreading and observed earthquake focal mechanisms shows an excellent agreement, both with regards to
220 stress regime and orientation of maximum compressive stress. The earthquake focal mechanisms are mostly
221 normal along the spreading ridges and strike-slip along the transform faults, and the focal mechanism pressure
222 axes align nicely with the predicted directions of maximum compressive stress (Fig. 3). The good agreement
223 between Okada's model and other modelling approaches as well as between the resulting stresses and focal
224 mechanisms in the area indicates that the model, despite the simplicity of its assumptions, provides a correct first
225 order prediction of orientation and type of the stress field in the upper crust (other possible sources of stress in the
226 region will be discussed in more detail in section 6.1). It remains an open question to which degree the crustal
227 stresses are transferred to the sedimentary successions of the Vestnesa Ridge. For compacted stratigraphic
228 formations in the Norwegian Sea, a comparison of shallow in-situ stress measurements and deeper observations
229 from earthquake focal mechanisms indicates that the stress field is homogeneous in direction over a large depth
230 range (Fejerskov and Lindholm, 2000). For an overburden constituted of Quaternary sediments, though, the stress
231 coupling between the crust and the near-surface depends on the shear strength of the sediments. The upper 200 m
232 of hemipelagic sediment along the Vestnesa Ridge are relatively young (< 2 Ma) and the degree of sediment
233 consolidation remains uninvestigated. However, the fact that a large number of faults extend several hundred
234 meters through the sediments suggests that compaction of the sediments has been large enough to build up some
235 amount of shear strength. Geotechnical studies from different continental margins indicate that deep marine
236 sediments can experience high compressibility due to the homogeneity in the grain structure (i.e., large areas
237 made of a single type of sediment), providing favourable conditions for shear failure (Urlaub et al., 2015; DeVore
238 and Sawyer, 2016). Therefore, we consider possible that the upper sedimentary column along the Vestnesa Ridge
239 has been deformed by tectonic stress.

240

241 **5.2 Distribution of faults and seepage activity along the Vestnesa Ridge with respect to modelled tectonic** 242 **stress**

243 High-resolution 3D seismic data collected on the eastern Vestnesa Ridge revealed sub-seabed NW-SE oriented,
244 near-vertical faults with a small normal throw (< 10 m; Fig. 5). In this part of the Vestnesa Ridge, gas chimneys
245 and seafloor pockmarks are ca. 500 m in diameter. On structural maps extracted along surfaces within the GHSZ
246 gas chimneys project over fault planes or at the intersection between fractures (Fig. 2, 3c). A set of N-S to NNE-
247 SSE trending faults outcrop at the seafloor at a narrow zone between the Vestnesa Ridge and the northern
248 termination of the Knipovich Ridge (Fig 1, 2). These faults have been suggested to indicate ongoing northward

249 propagation of the Knipovich rift system (Crane et al., 2001; Vanneste et al., 2005). The NW-SE oriented sub-
250 seabed faults and fractures at the crest of the Vestnesa Ridge could be genetically associated with these
251 outcropping faults (Plaza-Faverola et al., 2015; Fig. 2).

252

253 Most of the outcropping N-S to NNE-SSE oriented faults north of the Knipovich Ridge and the sub-seafloor NW-
254 SE oriented faults on the eastern Vestnesa Ridge are located within the zone of modelled tensile regime that
255 extends northward from the Knipovich Ridge (Fig. 3). The orientation of σ_H rotates from being perpendicular to
256 the Molloy ridge nearby sub-seafloor faults at the eastern Vestnesa Ridge, to be more perpendicular to the
257 Knipovich Ridge in places within the tensile zone (Fig. 3). Interestingly, documented acoustic flares along the
258 Vestnesa Ridge are also located within the zone of modelled tensile stress regime (Fig. 3). The match between the
259 extent of the modelled tensile regime and the active region of pockmarks is not exact; pockmarks with acoustic
260 flares exist a few kilometres westward from the termination of the tensile zone (Fig. 3). However, the agreement
261 is striking from a regional point of view. Some of the outcropping faults north of the Knipovich Ridge and south
262 of the Molloy transform fault appear located outside the modelled tensile zone (Fig. 3; Fig. S1-S4 in the
263 supplement). Inactive pockmarks (i.e., no acoustic flares have been observed during several visits to the area) are
264 visible on high resolution bathymetry maps over these faulted regions (Dumke et al., 2016; Hustoft, 2009; Johnson
265 et al., 2015; Waghorn et al., 2018).

266

267 In a similar high-resolution 3D seismic data set from the western Vestnesa Ridge the faults have different
268 characteristics compared to those of the eastern segment. In this part of the ridge gas chimneys are narrower,
269 buried pockmarks are stacked more vertically than the chimneys towards the east and it is possible to recognise
270 more faults reaching the present-day seafloor (Plaza-Faverola et al., 2015). Fault segments are more randomly
271 oriented with a tendency for WNW-ESE and E-W orientations (Fig. 2). These structures coincide with a
272 modelled strike-slip stress regime with σ_H oriented nearly perpendicular to the Molloy Ridge (Fig. 3).

273

274 **6. Discussion**

275 The striking coincidence between the spatial variation in modelled stress regimes and the pattern of faulting and
276 seepage activity along the Vestnesa Ridge leads to the discussion whether tectonic stresses resulting from plate
277 spreading at the Molloy and the Knipovich ridges have the potential to influence near-surface deformation and
278 fluid dynamics in the study area. We discuss first the modelling results in the context of the total state of stress
279 across passive margins and to which extent regional stresses can influence near-surface deformation. Assuming

280 that tectonic stress can potentially influence near-surface deformation, we discuss then the effect that the
281 modelled stress fields would have on pre-existing faults and associated fluid migration. Finally, we propose a
282 model for explaining seepage evolution along the Vestnesa Ridge coupled to stress field variations. We close the
283 discussion with a note on the implications of the present study for understanding near-surface fluid dynamics
284 across passive margins globally.

285

286 **6.1 Modelled stress in the context of the state of stress along the Vestnesa Ridge**

287 In this study we focused exclusively on modelling the type and orientation of stresses potentially generated by
288 spreading at the Molloy and Knipovich ridges. Other sources of stress have been so far disregarded. Hence, the
289 modelled stress field documented in this study cannot be considered as a representation of the total stress field in
290 the region. Modelling studies from Atlantic-type passive margins, suggest that from all the possible sources of
291 stress across passive margins (i.e., sediment loading, glacial flexure, spatial density contrasts, and ridge push as
292 well as basal drag forces) sediment loading (assuming elastic deformation) appears to be the mechanism with the
293 potential of generating the largest magnitudes of stresses across passive margins (Stein et al., 1989; Turcotte et al.,
294 1977). However, stress information derived from seismological and in-situ data (Fjeldskaar and Amantov,
295 2018; Grunnaleite et al., 2009; Lindholm et al., 2000; Olesen et al., 2013) and paleo-stress field analyses based on
296 dip and azimuth of fault planes (Salomon et al., 2015) point towards a dominant effect of ridge push forces on the
297 state of stress across passive continental margins. Given the proximity of the Vestnesa Ridge to the Molloy and
298 the Knipovich ridges (Fig. 1), we argue that tectonic stress from spreading can be an important factor, perhaps
299 even a dominant factor, controlling near-surface deformation along the Vestnesa Ridge.

300

301 The contemporary stress field across the west-Svalbard passive margin is presumably the result of an interaction
302 between large-scale tectonic stress mechanisms (i.e., ridge push, basal drag) overprinted by regional (i.e., density
303 contrasts, glacial related flexure, sediment loading) and local mechanisms (e.g., topography, pore-fluid pressure
304 variations, faulting). In the concrete case of the Vestnesa Ridge, a change in the faulting pattern, the distribution
305 of shallow gas and gas hydrates, as well as differences in the topographic characteristics of the ridge crest (Fig. 2,
306 5), are all factors likely to induce local changes in the degree of compaction and in near-surface stress. We
307 discuss in the following sections how local stress-generating mechanisms may interact with tectonic forcing to
308 control fluid dynamics and seepage.

309

310 The Vestnesa sedimentary Ridge sits over relatively young oceanic crust, < 19 Ma old (Eiken and Hinz,
311 1993;Hustoft, 2009). The oceanic-continental transition is not well constrained but its inferred location crosses
312 the Vestnesa Ridge at its easternmost end (Engen et al., 2008;Hustoft, 2009). This is a zone prone to flexural
313 subsidence due to cooling during the evolution of the margin and the oceanic crust may have experienced syn-
314 sedimentary subsidence focused around the oceanic-continental transition, as suggested for Atlantic passive
315 margins (Turcotte et al., 1977). However, syn-sedimentary subsidence would result in N-S oriented faults (i.e.,
316 reflecting the main direction of major rift systems during basin evolution) (Faleide et al., 1991;Faleide et al.,
317 1996). Although one N-S oriented fault outcrops in bathymetry data at the transition from the eastern to the
318 western Vestnesa Ridge segments (Fig. 5a), most of the sub-seabed faults and associated fluid migration features
319 in 3D seismic data are NW-SE to E-W oriented (Fig. 1, 2).

320

321 The weight of the contourite ridge over the oceanic crust may have generated additional stress on the Vestnesa
322 Ridge. Sedimentation rates on the Vestnesa Ridge have been moderate, estimated to have fluctuated between 0.1-
323 0.6 mm/year since the onset of glaciations 2.7 Ma ago (Plaza-Faverola et al., 2017;Knies et al., 2018;Mattingsdal
324 et al., 2014). The lithology of the upper sediment along the ridge appears dominated by soft fine-grained
325 hemipelagic clayey silt with variable concentrations of ice-rafted debris (Szybor and Rasmussen, 2017a).
326 Together, sedimentation rates and a high clay content would provide an ideal setting for undercompaction due to
327 increased pore fluid pressure (e.g., Fertl, 1976;Smith, 1999). High pore fluid pressure would lead to a decrease in
328 the effective stress and favour shearing (Grauls and Baleix, 1994). Whether these sedimentation rates have
329 allowed stress to build up through the upper strata faster than what it relaxes at the crust (i.e., as expected for
330 sedimentation rates larger than 1 mm/year (Stein et al., 1989)), as well as what has been the role of gas hydrates
331 and authigenic carbonate on the compaction history of the sediment remains to be investigated.

332

333 Glacial isostasy results in significant stresses associated with flexure of the lithosphere as the ice-sheet advances
334 or retreats. Present uplift rates are highest at the centre of the formerly glaciated region where the ice thickness
335 was at the maximum (Fjeldskaar and Amantov, 2018). Modelled present day uplift rates at the periphery of the
336 Barents sea ice-sheet ranges from 0 to -1 mm/year, depending on the ice-sheet model used in the calculation
337 (Auriac et al., 2016). This compares to an uplift rate of up to 9 mm/year at the centre of the ice sheet (Auriac et
338 al., 2016;Patton et al., 2016). Modelled glacial stresses induced by the Fennoscandian ice sheet on the mid-
339 Norwegian margin are close to zero at present day (Lund et al., 2009;Steffen et al., 2006). By analogy, present
340 day stress along the Vestnesa Ridge - located ~60 km from the shelf break - may be insignificant. It is likely that

341 glacial stresses as far off as the Vestnesa Ridge had a more significant effect in the past, as further discussed in
342 section 6.3 and 6.4.

343
344 Finally, ridge push forcing has the potential of being a dominant factor on the state of stress across the west-
345 Svalbard margin as observed for Norwegian margins (Fejerskov and Lindholm, 2000;Lindholm et al., 2000).
346 Specifically, the Vestnesa Ridge has the particularity that it is located within the expected range of maximum
347 influence of ridge push forces on the stress regime (Fejerskov and Lindholm, 2000) and that forces from two
348 spreading ridges influence it from different directions (i.e., the Molloy Ridge from the west and the Knipovich
349 Ridge from the south-east). The intriguing stress pattern appears to be caused by the interaction of the stress
350 generated by the two spreading ridges, as described above (section 5.1).

351 352 **6.2 Effect of the modelled stress fields on pre-existing faults and present day seepage**

353 Bearing in mind that several factors contribute to the total state of stress at different scales across passive margins
354 we assume that an influence on near-surface deformation by mid-ocean ridge stresses is plausible and discuss
355 their potential effect on seepage activity. Depending on the tectonic regime, the permeability through faults and
356 fractures may be enhanced or inhibited (e.g., Sibson, 1994;Hillis, 2001;Faulkner et al., 2010). Thus, spatial and
357 temporal variations in the tectonic stress regime may control the transient release of gas from the seafloor over
358 geological time as documented, for example, for CO₂ analogues in the Colorado Plateau (e.g., Jung et al., 2014).

359
360 A gas hydrate system is well developed and shallow gas accumulates at the base of the GHSZ along the entire
361 Vestnesa Ridge (Plaza-Faverola et al., 2017). Thermogenic gas accumulations at the base of the GHSZ (Fig. 5)
362 are structurally controlled (i.e., the gas migrates towards the crest of the sedimentary ridge) and together with
363 microbial methane this gas sustains present day seepage activity (Bünz et al., 2012;Plaza-Faverola et al.,
364 2017;Knies et al., 2018). However, seepage is focused and restricted. Some of the mechanisms commonly
365 invoked to explain seepage activity across passive margins include climate related gas hydrate dissociation, tidal
366 or seasonal sea-level changes, and pressure increases in shallow reservoirs due to fast sedimentation (e.g., Bünz
367 et al., 2003;Hustoft et al., 2010;Karstens et al., 2018;Riboulot et al., 2014;Skarke et al., 2014;Berndt et al.,
368 2014;Wallmann et al., 2018;Westbrook et al., 2009;Franek et al., 2017). While all of these mechanisms may
369 influence seepage systems as deep as the Vestnesa Ridge (> 1000 m deep; as discussed further in section 6.3)
370 they offer no explanation as to why seepage activity is more substantial within chimney sites proximal to or at
371 fault planes and why seepage is at a minimum or stopped elsewhere along the ridge (Fig. 2, 5). Overall, the

372 pattern of seepage activity along the Vestnesa Ridge is strikingly consistent with the modelled tectonic stress
373 field pattern. Acoustic flares have been documented to originate from < 10 m broad zones (Panieri et al., 2017)
374 within pockmarks located exclusively along faults. We suggest that these faults are favourably oriented with
375 respect to a tectonic σ_H (Fig. 2) and that opening of fault segments favourably oriented with respect to the stress
376 field is one controlling factor of present day seepage.

377

378 Present day seepage activity is less pronounced towards the western Vestnesa Ridge. Despite available gas
379 trapped at the base of the GHSZ (Fig. 5) the faults are generally less favourably oriented for tensile opening (i.e.,
380 NW-SE oriented σ_H) and are under a strike-slip regime (Fig. 2). The cluster of larger scale N-S to NNW-SSE
381 trending extensional faults that outcrop at the southern slope of the Vestnesa Ridge (Fig. 1, 2), also coincides
382 with the zone of predicted tensile stress (Fig. 3). However, the modelled maximum compressive stress in this area
383 is generally oblique to the fault planes, making these faults less open for gas. Interestingly, this is also a zone of
384 pockmarks where acoustic flares have not been observed (e.g., Johnson et al., 2015; Hustoft et al., 2009;
385 Vanneste et al., 2005). A set of N-S oriented structures south of the Molloy Transform Fault and a train of
386 pockmarks at the crest of a ridge west of the Knipovich Ridge axis are located under a strike-slip regime with N-
387 S oriented σ_H (Fig. 3). Although gas accumulations and gas hydrates have been identified at the crest of this ridge,
388 acoustic flares have so far not been documented (Johnson et al., 2015; Waghorn et al., 2018). We suggest that the
389 N-S trending faults in this region may be impermeable for fluids despite a parallel σ_H , if the stress regime is
390 transpressive. Transpression has been documented at different stages of opening of the Fram Strait (Jokat et al.,
391 2016; Myhre and Eldholm, 1988) and is thus a plausible tectonic mechanism for holding the gas from escaping.
392 Ongoing studies will shed light into the structural evolution of this near-surface system.

393

394 The bathymetry of the southern flank of the Vestnesa Ridge deepens from 1200-1600 m along the crest of the
395 Vestnesa Ridge to ca. 2000 m near the Molloy Transform Fault (Fig. 1). Thus, an additional effect of
396 gravitational stress on near-surface deformation and seepage in the region cannot be ruled out. In particular,
397 although the faults at the steep slope north of the Knipovich Ridge have been suggested to reflect the northward
398 propagation of the Knipovich Ridge rift system (Crane et al., 2001; Vanneste et al., 2005), it is likely that their
399 formation was influenced by gravitational stresses. Small-scale slumps at the slope (Fig 1, 2) could be also
400 evidence of gravitational forcing at the steep southern flank of the Vestnesa Ridge. However, sub-seabed faults
401 on the eastern Vestnesa Ridge dip towards the NE (Fig. 5c), suggesting that gravitational forcing is not
402 necessarily influencing the behaviour of faults and current seepage activity on the eastern Vestnesa Ridge.

403

404 **6.3 Seepage evolution coupled to stress field variations**

405 The seepage systems along the Vestnesa Ridge has been highly dynamic over geological time. Both microbial
406 and thermogenic gas contribute to the gas hydrate and seepage system (Hong et al., 2016;Panieri et al.,
407 2017;Plaza-Faverola et al., 2017;Smith et al., 2014). Reservoir modelling shows that source rock deposited north
408 of the Molloy Transform Fault has potentially started to generate thermogenic gas 6 Ma ago and that migrating
409 fluids reached the Vestnesa Ridge crest at the active seepage site ca. 2 Ma ago (Knies et al., 2018). Seepage has
410 been occurring, episodically, at least since the onset of the Pleistocene glaciations directly through faults, and a
411 deformation typical of gas chimneys (i.e., where periodicity is evidenced by buried pockmarks and authigenic
412 carbonate crusts) seems to have started later (Plaza-Faverola et al., 2015). However, the periodicity of seepage
413 events documented since the Last Glacial Maximum seems to correlate indistinctively with glacials or
414 interglacials (Consolaro et al., 2015;Schneider et al., 2018a;Szybor and Rasmussen, 2017b). One transient event
415 was dated to ca. 17.000 years based on the presence of a ~1000 years old methane-dependent bivalve community
416 possibly sustained by a gas pulse through a fault or chimney (Ambrose et al., 2015). A tectonic control on the
417 evolution of near-surface fluid flow systems and seepage along the Vestnesa Ridge is an explanation that
418 reconciles the numerous cross-disciplinary observations in the area.

419

420 The spatial relation between gas chimneys at the crest of the ridge and fault planes (Fig. 2, 5c) (Bünz et al.,
421 2012;Plaza-Faverola et al., 2015) is intriguing and raises the question whether the faulting was posterior to
422 brecciation (fracturing) of the strata during chimney formation. Gas chimneys form by hydrofracturing generated
423 at a zone of overpressure in a reservoir (e.g., Karstens and Berndt, 2015;Hustoft et al., 2010 and references
424 therein;Davies et al., 2012). From the mechanical point of view the tensile faults at the eastern Vestnesa Ridge
425 would not be a favourable setting for the generation of hydrofracturing and chimney formation right through fault
426 planes as observed in the seismic (Fig. 2, 5c). For gas chimneys to be the youngest features fault segments would
427 have to become tight and permeable at certain periods of times, allowing pore fluid pressure e.g., at the free gas
428 zone beneath the GHSZ to build up (Fig. 5). This is a plausible scenario. The faults may get locally plugged with
429 gas hydrates and authigenic carbonate and activate a self-sealing mechanism similar to that suggested for
430 chimneys at other margins (e.g., Hovland, 2002). A model of gas hydrate-sealed faults and increased free gas
431 zone underneath, has been suggested to explain seismic attenuation and velocities from an ocean bottom seismic
432 experiment over the gas hydrate system north of the Knipovich Ridge (Madrussani et al., 2010). Nevertheless,
433 where gas chimneys do not disturb the seismic response, fault planes are observed to extend near the seafloor

434 (Fig. 5c). This observation suggests that latest faulting periods may have broken through already brecciated
435 regions connecting gas chimneys that were already in place. Both cases are consistent with the fact that acoustic
436 flares and seepage bubbles are restricted to focused weakness zones (Panieri et al., 2017). We suggest that an
437 interaction between pore fluid pressure at the base of the GHSZ and tectonic stress has led to local stress field
438 variations and controlled seepage evolution. Opening of fractures is facilitated if the minimum horizontal stress is
439 smaller than the pore-fluid pressure (p_f), that is, the minimum effective stress is negative ($\sigma_h' = \sigma_h - p_f < 0$) (e.g.,
440 Grauls and Baleix, 1994). Secondary permeability may increase by formation of tension fractures near damaged
441 fault zones (Faulkner et al., 2010). Cycles of negative minimum effective stress and subsequent increase in
442 secondary permeability in a tensile stress regime can be achieved particularly easy in the near-surface and would
443 provide an explanation for the development of chimneys coupled to near-surface tectonic deformation. A
444 constant input of thermogenic gas from an Eocene reservoir since at least ca. 2 Ma ago would have contributed to
445 localized pore-fluid pressure increases (Knies et al., 2018).

446

447 Geophysical and paleontological data indicate that there was once more prominent seepage and active chimney
448 development on the western Vestnesa Ridge segment (e.g., Consolaro et al., 2015; Plaza-Faverola et al.,
449 2015; Schneider et al., 2018b). An interaction between pore-fluid pressure and tectonic stress would explain
450 variations in the amount of seepage activity over geological time. Following the same explanation as for the
451 present day seepage, the negative σ_h' condition could have been attained anywhere along the Vestnesa Ridge in
452 the past due to pore fluid pressure increases at the base of the GHSZ or due to favourable stress conditions.
453 During glacial periods, flexural stresses should have been significantly higher than at present day (Lund and
454 Schmidt, 2011). According to recent models of glacial isostasy by the Barents Sea Ice sheet during the last glacial
455 maximum, the Vestnesa Ridge laid in a zone where subsidence could have been of tens of meters (Patton et al.,
456 2016). At other times, before and after glacial maximums, the Vestnesa Ridge was possibly located within the
457 isostatic forebulge.

458

459 In general, it is expected that glacial-induced maximum horizontal stresses (σ_H) would be dominantly oriented
460 parallel to the shelf break (Björn Lund personal communication; Lund et al., 2009), that is, oriented N-S in the
461 area of the Vestnesa Ridge (Fig. 1). Such stress orientation would not favour opening for fluids along pre-existing
462 NW-SE oriented faults associated with seepage activity at present (i.e., N-S oriented faults would be the more
463 vulnerable for opening). It is possible, though, that the repeated waxing and waning of the ice sheet caused a
464 cyclic modulation of the stress field (varying magnitude and orientation) and influenced the dynamics of gas

465 accumulations and favourably oriented faults along the Vestnesa Ridge in the past. Past glacial stresses may
466 provide then an alternative explanation for seepage along the entire Vestnesa Ridge extent at given periods of
467 time (Fig. 6). This explanation is in line with the correlation between seepage and glacial-interglacial events
468 postulated for different continental margins e.g., for chimneys off the mid-Norwegian margin (Plaza-Faverola et
469 al., 2011), the Gulf of Lion (Riboulot et al., 2014), but also along the Vestnesa Ridge (Plaza-Faverola et al.,
470 2015;Schneider et al., 2018b).

471

472 A temporal variation in the stress field along the Vestnesa Ridge is also caused by its location on a constantly
473 growing plate. As the oceanic plate grows, the Vestnesa Ridge moves eastward with respect to the Molloy and
474 Knipovich Ridges, causing a westward shift in the regional stress field on the Vestnesa Ridge (Fig. 7). In future,
475 the eastern Vestnesa Ridge may temporarily move out of the tensile zone, while the western Vestnesa Ridge
476 moves into it (Fig. 7). This suggests that a negative effective stress and subsequent active seepage may reappear
477 and “reactivate” pockmarks to the west of the currently active seepage zone.

478

479 **6.4 Implications for the understanding of near-surface deformation across passive margins**

480 Our study is a first step in the investigation of the effect of regional stress on the dynamics of near-surface fluid
481 flow systems across passive margins. Analytical modelling of spreading at the Molloy and the Knipovich ridges
482 shows that complex stress fields may arise from the interaction of the dynamics at plate boundaries and exert an
483 effect across passive margins. Although the Vestnesa Ridge is a unique case study due to its remarkable
484 proximity to the Arctic mid-ocean ridges, stresses generated by plate tectonic forces are expected to extend for
485 thousands of km (Fejerskov and Lindholm, 2000). Across a single passive margin a range of regional and local
486 factors may result in spatial stress field variations that can explain focusing of gas seepage at specific regions. For
487 instance, the pervasive seepage zone west of Prins Karls Forland (PKF) on the west-Svalbard margin (Fig. 1)
488 could be under a stress regime that has been influenced by glacial rebound at a larger degree than at the Vestnesa
489 Ridge area over geological time. Wallmann et al., (2018) suggested that post glacial uplift lead to gas hydrate
490 dissociation after the Last Glacial Maximum and that such gas continues to sustain seepage off PKF. Previously,
491 several other studies argued for a gas-hydrate control on seepage in this region (e.g., Berndt et al., 2014;Portnov
492 et al., 2016;Westbrook et al., 2009). Since no gas hydrates have been found despite deep drilling (Riedel et al.,
493 2018) the gas hydrate hypotheses remain debatable. The influence of regional stresses on sub-seabed faults
494 suspected to underlay the seepage system (e.g., Mau et al., 2017) and shallow gas reservoirs (Knies et al., 2018)
495 provides an alternative and previously not contemplated explanation for seepage in this area. The interactions

496 between tectonic stress regimes and pore-fluid pressure we propose for explaining seepage evolution along the
497 Vestnesa Ridge may be applicable to seepage systems along other passive margins, in particular along Atlantic
498 passive margins where leakage from hydrocarbon reservoirs is prominent (e.g., the mid-Norwegian margin, the
499 Barents Sea, the North Sea, the north-east Greenland margin, the Mediterranean and even the Scotia plate
500 between Argentina and Antarctica) (e.g., Andreassen et al., 2017;Bünz et al., 2003;Hovland and Sommerville,
501 1985;Riboulot et al., 2014;Somoza et al., 2014;Vis, 2017). The Vestnesa Ridge case study adds a new perspective
502 to the current debate about the inactivity of passive margins (Fejerskov and Lindholm, 2000;Fjeldskaar and
503 Amantov, 2018;Lindholm et al., 2000;Olesen et al., 2013;Stein et al., 1989).

504

505 **7. Conclusions**

506 Analytical modelling of the stress field generated by oblique spreading at the Molloy and Knipovich ridges in the
507 Fram Strait, suggests that spatial variations in the tectonic stress regime along the Vestnesa Ridge are plausible.
508 Thus, mid-ocean ridge spreading may be an important factor controlling faulting and seepage distribution in the
509 region. Other important sources of stress such as gravitational forcing and lithospheric bending, contributing to
510 the actual state of stress off Svalbard, are not considered in the modelling exercise presented here. Hence, we
511 cannot quantitatively assess whether ridge push has a dominant effect on seepage activity. However, provided a
512 certain degree of coupling between crustal and near-surface deformation, it is plausible that stresses from plate
513 spreading may affect the behaviour of Quaternary faults along the Vestnesa Ridge and exert a certain control on
514 seepage. Our study supports a tectonic explanation for the observed seepage pattern in the region. The influence
515 of rifting at the Knipovich Ridge dominantly on the eastern Vestnesa Ridge may be the key for understanding
516 focusing of present day seepage activity along the ridge. The opening of faults and fractures favourably oriented
517 with respect to principal stresses combined with a diminished effective stress in a tensile stress regime facilitates
518 the release of gas from zones of relatively high-pore fluid pressure at the base of the gas hydrate stability zone.
519 Multiple seepage events along the entire extent of the Vestnesa Ridge, may have been induced by additional
520 sources of stress likely associated with glacial isostasy. Future reactivation of currently dormant pockmarks or
521 increase in seepage activity is likely following the gradual westward propagation of the tensile stress zone on the
522 Vestnesa Ridge as the Eurasian plate drifts towards the south-east. Despite the simplifying assumptions by the
523 analytical model approach implemented here, this study provides a first assessment of how important
524 understanding the state of stress is for reconstructing seepage activity along passive margins.

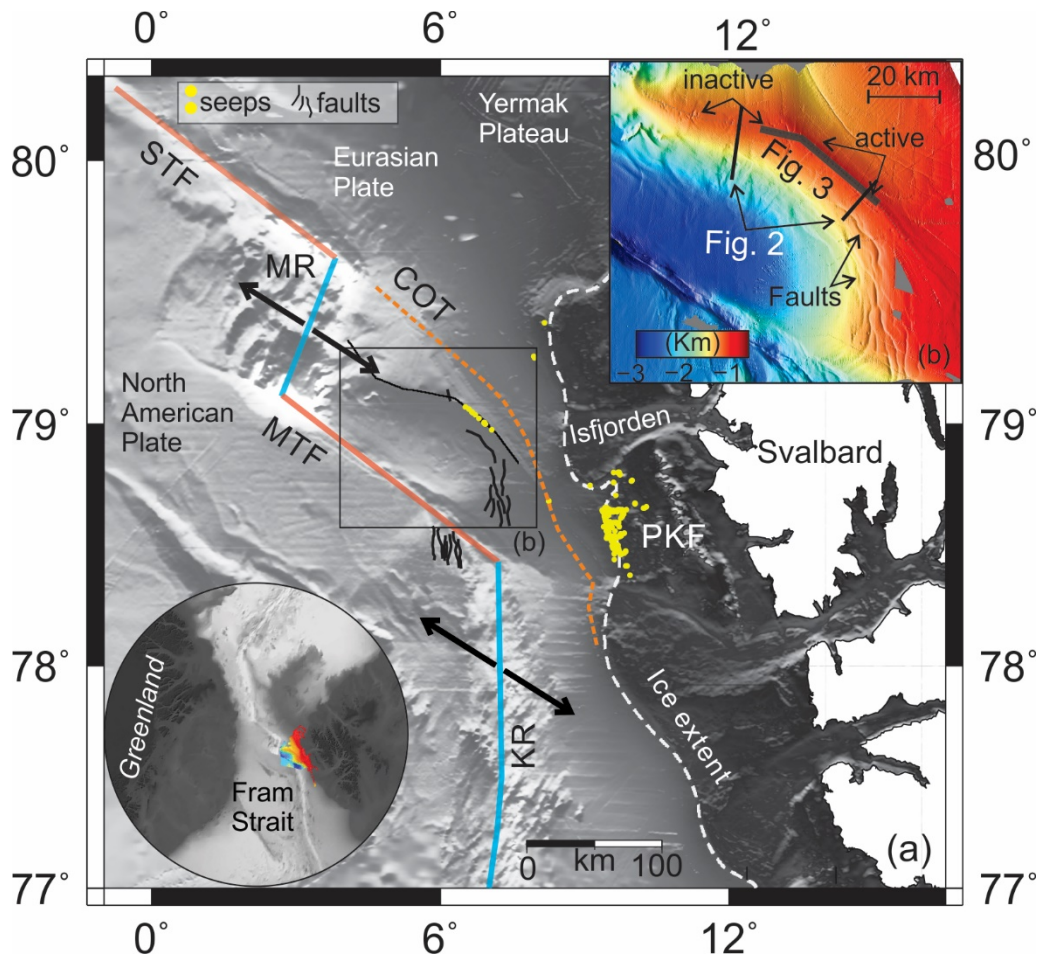
525

526 **8. Outlook**

527 The effect of glacial stresses over the fluid flow system off west-Svalbard will be further tested (at least for the
 528 Weichselian period) by implementing Lund et al., models using newly constrained Barents Sea ice-sheet models
 529 (e.g., Patton et al., 2016). Additional sources of stress related to topography/bathymetry should be further
 530 investigated as well to gain a comprehensive assessment of the effect of the total stress field on near-surface fluid
 531 migration in the region.

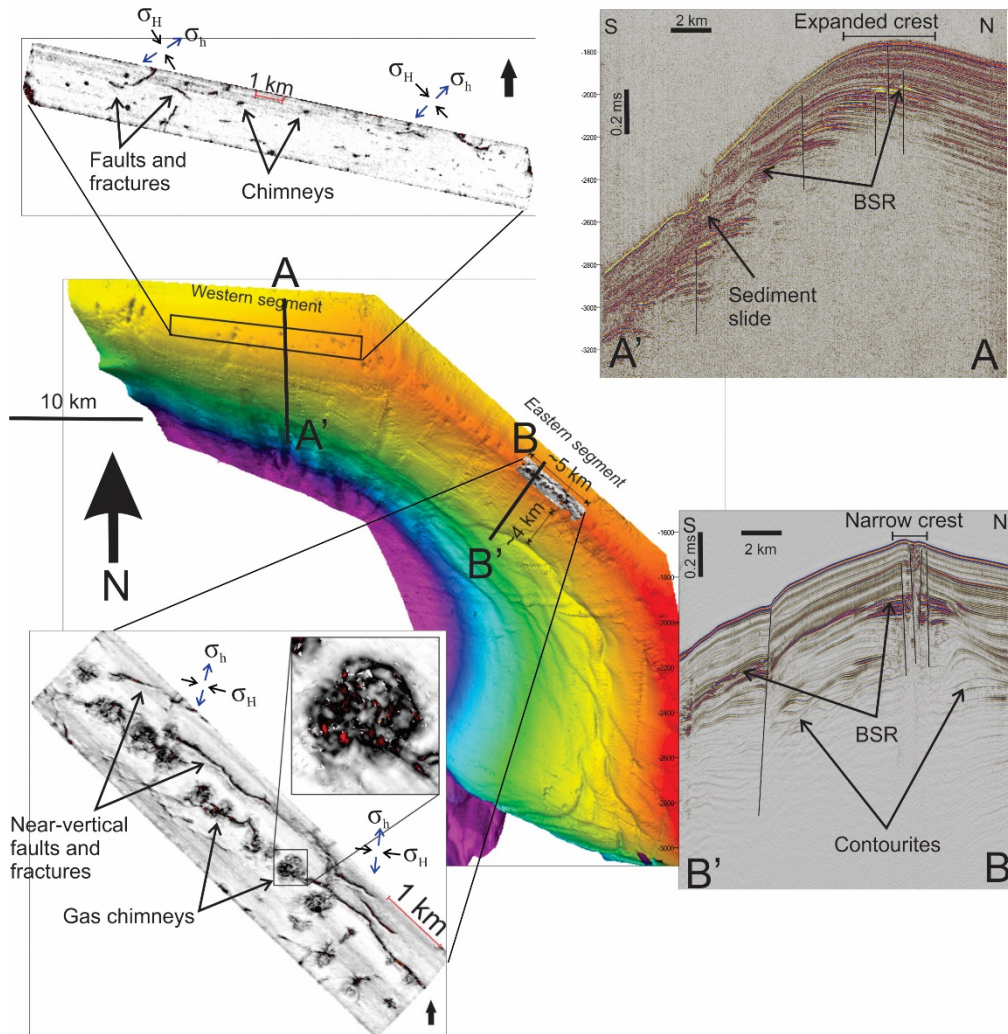
532 **Figures**

533



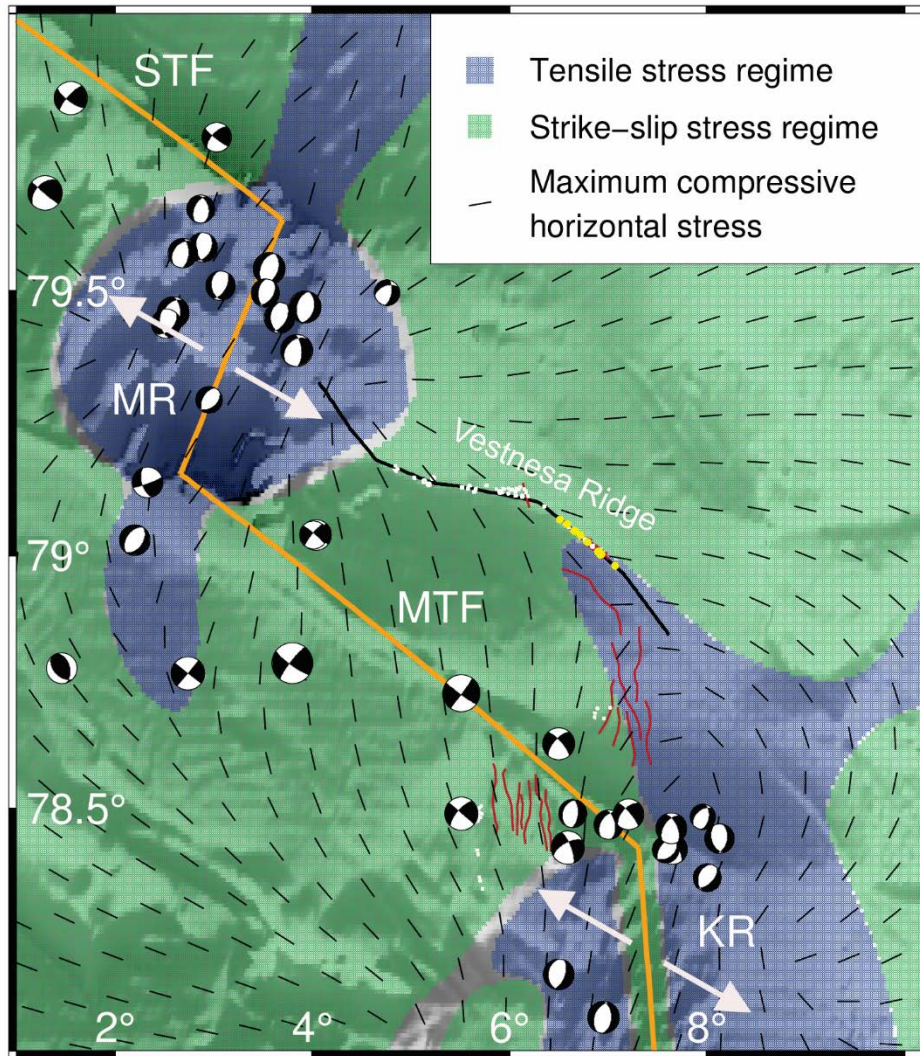
534
 535 **Figure 1: (a) International Bathymetry Chart of the Arctic Ocean (IBCAO) showing the geometry of mid-**
 536 **ocean ridges offshore the west-Svalbard margin; (b) High resolution bathymetry along the Vestnesa Ridge**
 537 **(UiT, R/V HH multi-beam system). Seafloor pockmarks are observed along the entire ridge but acoustic**
 538 **flares are restricted to the eastern segment; PKF=Prins Karls Forland; STF=Spitsbergen Transform**

539 Fault; MR=Molloy Ridge; MTF=Molloy Transform Fault; KR=Knipovich Ridge; COT=Continental-
540 Oceanic Transition (Engen et al., 2008); Ice-Sheet Extent (Patton et al., 2016).
541



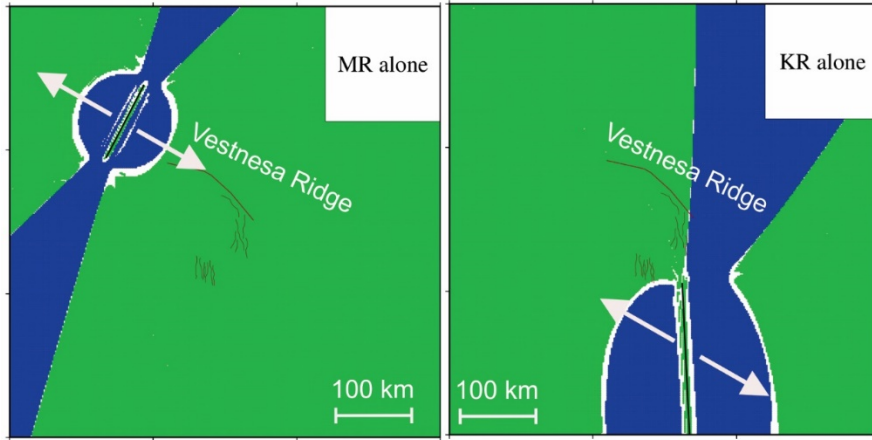
542
543 **Figure 2: Composite figure with bathymetry and variance maps from 3D seismic data along the eastern**
544 **and the western Vestnesa Ridge segments (modified from Plaza-Faverola et al., 2015). The orientation of**
545 **maximum compressive horizontal stress (σ_H) and minimum horizontal stress (σ_h) predicted by the model**
546 **are projected for comparison with the orientation of fault segments. Notice favourable orientation for**
547 **opening to fluids on the eastern Vestnesa Ridge segment. Two-2D seismic transects (A-A' - Bünz et al.,**
548 **2012 and B-B' – Johnson et al., 2015) illustrate the morphological difference of the crest of the Vestnesa**

549 Ridge (i.e., narrow vs. extended) believed to be determined by bottom current dominated deposition and
550 erosion (Eiken and Hinz, 1993). BSR=bottom simulating reflector.
551
552



553
554 **Figure 3: Modelled upper crustal tectonic stress field (blue – tensile and green - strike-slip regime) and**
555 **stress orientations, due to oblique spreading at the Molloy Ridge (MR) and the Knipovich Ridge (KR). The**
556 **outline of a seismic line (Plaza-Faverola et al., 2017) is projected as reference for the crest of the Vestnesa**
557 **Ridge. Red lines are faults, yellow dots seeps and white circles pockmarks where no acoustic flares have**

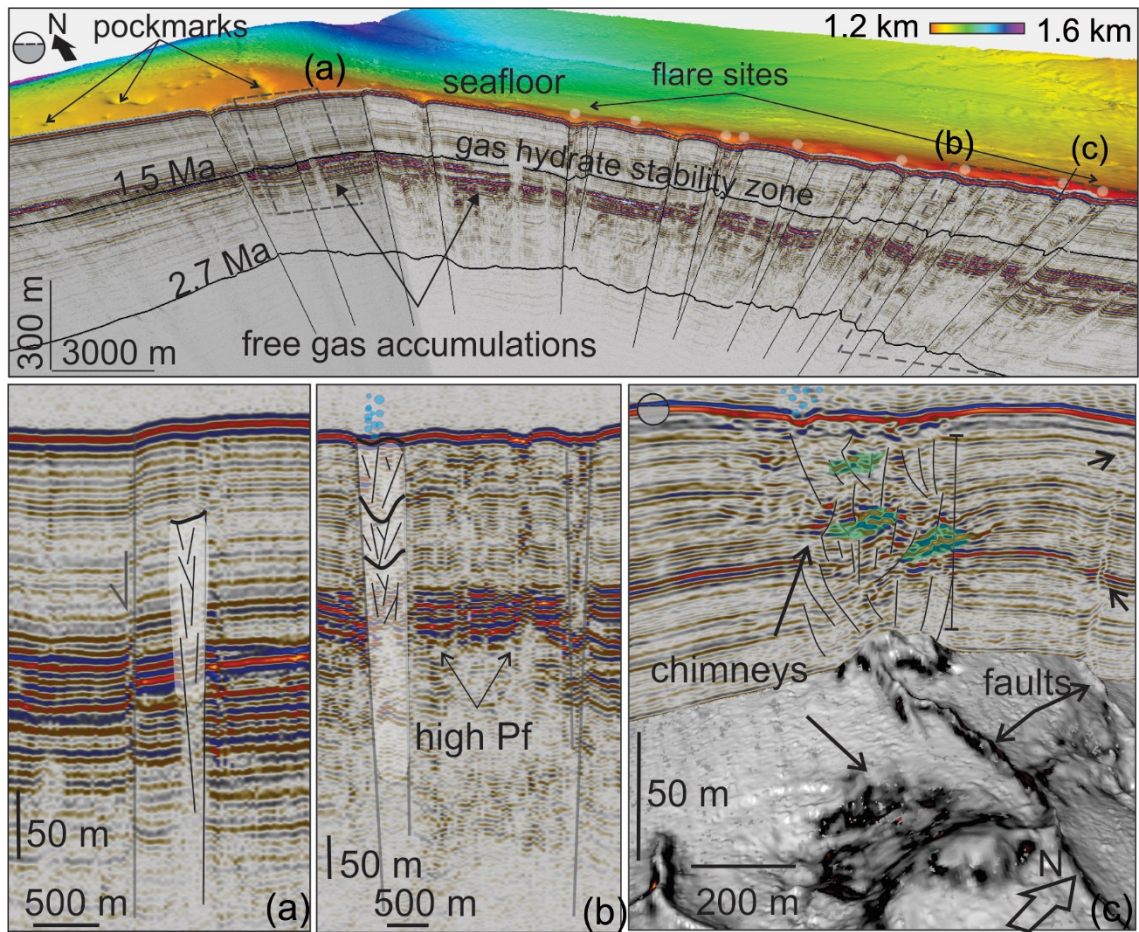
558 been documented. STF=Spitsbergen Transform Fault; MTF=Molloy Transform Fault. The focal
559 mechanisms are from the ISC Online Bulletin (<http://www.isc.ac.uk>).



560

561 **Figure 4: Stress field resulting from model runs with Molloy Ridge and Knipovich Ridge, respectively:**
562 **tensile stress field (blue); strike-slip stress field (green).**

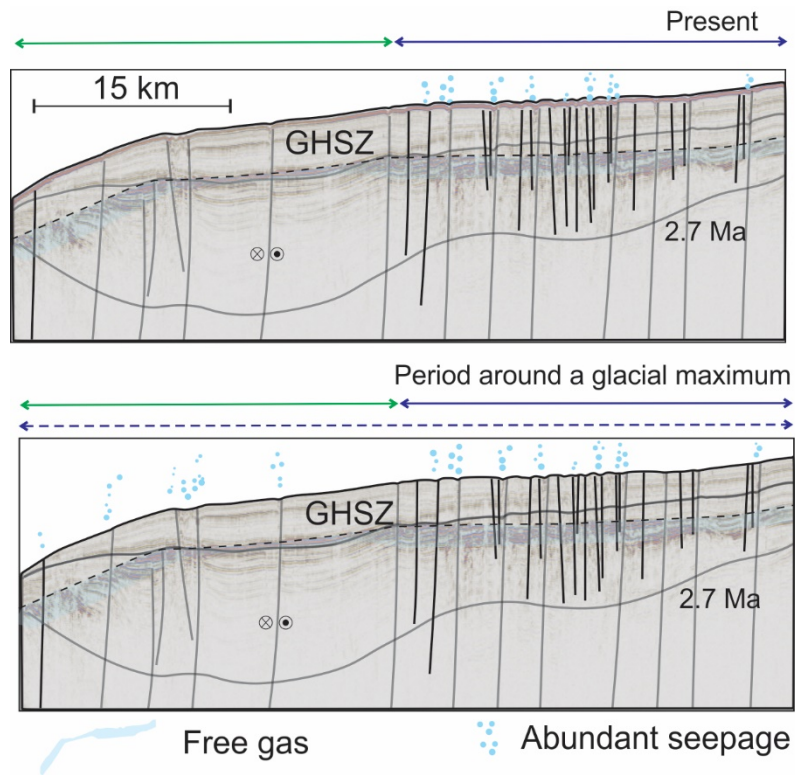
563



564

565 **Figure 5: Integrated seismic and bathymetry image of the gas hydrate system along the Vestnesa Ridge. (a)**
 566 **Outcropping N-S oriented fault located at the transition from the region where acoustic flares have been**
 567 **documented to the region where no flares have been observed; (b) Gas chimneys with associated acoustic**
 568 **flare and inferred high pore-fluid pressure (Pf) zone at the base of the gas hydrate stability zone; (c) Gas**
 569 **chimney associated with faults and faults extending to near-surface strata without being associated with**
 570 **chimneys. The same variance map in figure 2 is projected at the depth where the map was extracted along**
 571 **a surface interpreted on the 3D seismic volume. Green patches represent interpreted zones of buried**
 572 **authigenic carbonate that can activate a self-sealing mechanism leading to hydrofracturing and chimney**
 573 **development.**

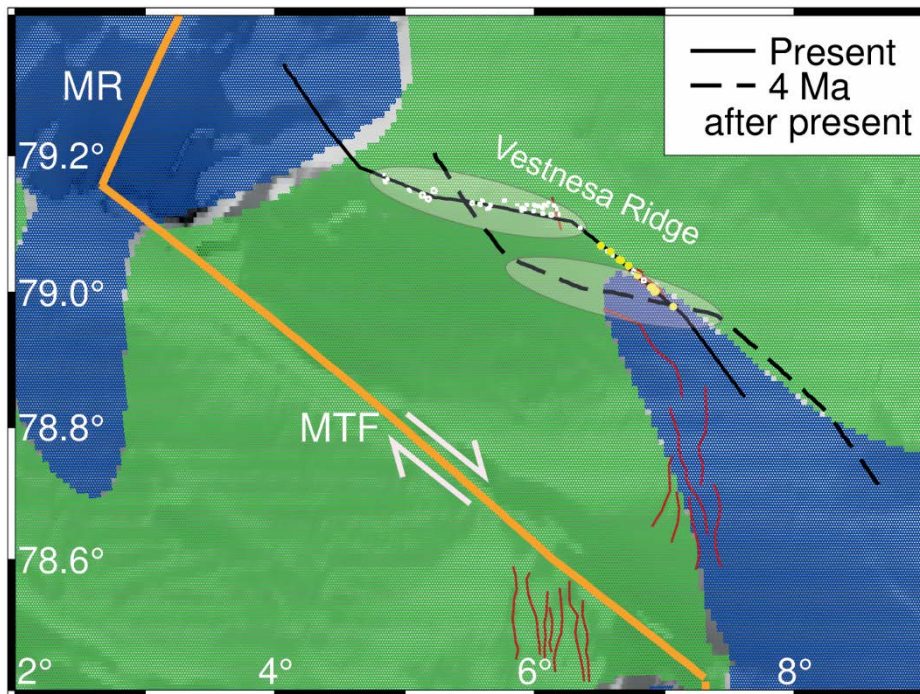
574



575

576 **Figure 6: Conceptual model of the evolution of seepage coupled to faulting and spatial variations in the**
 577 **stress regime (tensile=blue; strike-slip=green) along the Vestnesa Ridge, offshore the west-Svalbard**
 578 **margin. At present day, tensile stress from mid-ocean ridge spreading (blue solid line) favours seepage**
 579 **exclusively on the eastern segment of the Vestnesa Ridge. Seepage on the western Vestnesa Ridge and**
 580 **other regions may have been induced repeatedly since the onset of glaciations 2.7 Ma ago (Mattingsdal et**
 581 **al., 2014), due to tensional flexural stresses (dashed blue line) in the isostatic forebulge around the time of**
 582 **glacial maximums; GHSZ=gas hydrate stability zone. The dashed black line follows the bottom simulating**
 583 **reflector which represents the base of the GHSZ.**

584



585

586 **Figure 7: Stress field as in figure 3 showing the location of the Vestnesa Ridge at present and 4 Ma after**
 587 **present time, assuming a constant spreading velocity of 7 mm/yr in the direction N125°E. The same line**
 588 **outline as in figure 3 is used as reference for the crest of the Vestnesa Ridge. Yellow and white dots**
 589 **represent pockmarks with and without documented acoustic flares respectively.**

590

591 Appendix A

592 Model description

593

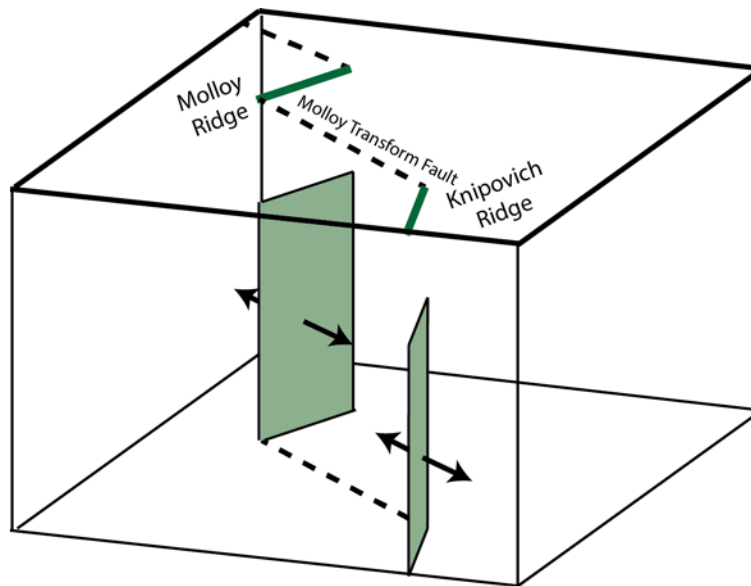
594 We use the analytical formulations of Okada (1985) for a finite rectangular dislocation source in elastic
 595 homogeneous isotropic half-space (Fig. A.1). The dislocation source can be used to approximate deformation
 596 along planar surfaces, such as volcanic dykes (e.g. Wright et al., 2006), sills (e.g. Pedersen and Sigmundsson,
 597 2004), faults (e.g. Massonet et al, 1993) and spreading ridges (e.g. Keiding et al., 2009). More than one
 598 dislocation can be combined to obtain more complex geometry of the source or varying deformation along a
 599 planar source. The deformation of the source can be defined as either lateral shear (strike-slip for faults), vertical
 600 shear (dip-slip at faults) or tensile opening.

601

602 The Okada model assumes flat Earth without inhomogeneities. While the flat-earth assumption is usually
603 adequate for regional studies (e.g. Wolf, 1984), the lateral inhomogeneities can sometimes cause considerable
604 effect on the deformation field (e.g. Okada, 1985). However, the dislocation model is useful as a first
605 approximation to the problem.

606

607 At mid-ocean ridges, deformation is driven by the continuous spreading caused by gravitational stress due to the
608 elevation of the ridges, but also basal drag and possibly slab pull. Deformation occurs continuously in the ductile
609 part of the crust. Meanwhile, elastic strain builds in the upper, brittle part of the crust. To model this setting, the
610 upper boundary of the dislocation source must be located at the depth of the brittle-ductile transition zone. The
611 lower boundary of the source is set to some arbitrary large depth to avoid boundary effects.



612

613 **Fig A.1 Extract of model showing the location of the dislocation sources (light green) for Molloy and**
614 **Knipovich ridges. Note that the model is an infinite half-space, i.e. it has no lateral or lower boundary.**

615

616 The Okada model provides the displacements u_x , u_y , u_z (or velocities if deformation is time-dependent) at defined
617 grid points at the surface and subsurface. It also provides strain (or strain rates) defined as:

618

$$\varepsilon_{ij} = \frac{1}{2}(u_{i,j} + u_{j,i})$$

619

620 The stress field can then be calculated from the predicted strain rates. In homogeneous isotropic media, stress is
621 related to strain as:

$$622 \quad \sigma_{ij} = \lambda \delta_{ij} \varepsilon_{kk} + 2\mu \varepsilon_{ij}$$

623
624 where δ_{ij} is the Kronecker delta, λ is Lamé's first parameter, and μ is the shear modulus. Lamé's first parameter
625 does not have a physical meaning but is related to the shear modulus and Poisson's ratio (ν) as $\lambda = \frac{2\mu\nu}{1-2\nu}$.

626
627 The absolute values of stress are in general difficult to model (e.g. Hergert and Heidbach, 2011), and not possible
628 with our analytical model. However, the model provides us with the orientations and relative magnitude of the
629 stresses. That is, we know the relative magnitudes between the vertical stress (σ_v), maximum horizontal stress
630 (σ_H) and minimum horizontal stress (σ_h). From this, the stress regime can be defined as either tensile ($\sigma_v > \sigma_H >$
631 σ_h), strike-slip ($\sigma_H > \sigma_v > \sigma_h$) or compressive ($\sigma_H > \sigma_h > \sigma_v$).

632

633 **Author contribution**

634 Andreia Plaza-Faverola conceived the paper idea. She is responsible for seismic data processing and
635 interpretation. Marie Keiding did the tectonic modelling. The paper is the result of integrated work between both.
636

637 **ACKNOWLEDGEMENTS**

638 This research is part of the Centre for Arctic Gas Hydrate, Environment and Climate (CAGE) supported by the
639 Research Council of Norway through its Centres of Excellence funding scheme grant No. 223259. Marie Keiding
640 is supported by the NEONOR2 project at the Geological Survey of Norway. Special thanks to Björn Lund, Peter
641 Schmidt, Henry Patton, and Alun Hubbard for their interest in the present project and constructive discussions
642 about isostasy and glacial stresses. We are thankful to various reviewers that have significantly contributed to the
643 improvement of the manuscript. Seismic data is archived at CAGE – Centre for Arctic Gas Hydrate, Environment
644 and Climate, Tromsø, Norway and can be made available by contacting APF. Modelled stresses can be made
645 available by contacting MK.

646

647 **References:**

648 Ambrose, W. G., Panieri, G., Schneider, A., Plaza-Faverola, A., Carroll, M. L., Åström, E. K., Locke, W. L., and
649 Carroll, J.: Bivalve shell horizons in seafloor pockmarks of the last glacial-interglacial transition: a thousand years
650 of methane emissions in the Arctic Ocean, *Geochemistry, Geophysics, Geosystems*, 16, 4108-4129, 2015.

651 Andreassen, K., Hubbard, A., Winsborrow, M., Patton, H., Vadakkepuliambatta, S., Plaza-Faverola, A.,
652 Gudlaugsson, E., Serov, P., Deryabin, A., and Mattingsdal, R.: Massive blow-out craters formed by hydrate-
653 controlled methane expulsion from the Arctic seafloor, *Science*, 356, 948-953, 2017.

654 Árnadóttir, T., Lund, B., Jiang, W., Geirsson, H., Björnsson, H., Einarsson, P., and Sigurdsson, T.: Glacial rebound
655 and plate spreading: results from the first countrywide GPS observations in Iceland, *Geophysical Journal
656 International*, 177, 691-716, 2009.

657 Auriac, A., Whitehouse, P., Bentley, M., Patton, H., Lloyd, J., and Hubbard, A.: Glacial isostatic adjustment
658 associated with the Barents Sea ice sheet: a modelling inter-comparison, *Quaternary Science Reviews*, 147, 122-
659 135, 2016.

660 Berndt, C., Feseker, T., Treude, T., Krastel, S., Liebetrau, V., Niemann, H., Bertics, V. J., Dumke, I., Dünnbier, K.,
661 and Ferré, B.: Temporal constraints on hydrate-controlled methane seepage off Svalbard, *Science*, 343, 284-287,
662 2014.

663 Bünz, S., Mienert, J., and Berndt, C.: Geological controls on the Storegga gas-hydrate system of the mid-
664 Norwegian continental margin, *Earth and Planetary Science Letters*, 209, 291-307, 2003.

665 Bünz, S., Polyanov, S., Vadakkepuliambatta, S., Consolaro, C., and Mienert, J.: Active gas venting through
666 hydrate-bearing sediments on the Vestnesa Ridge, offshore W-Svalbard, *Marine geology*, 2012.

667 Chand, S., Thorsnes, T., Rise, L., Brunstad, H., Stoddart, D., Bøe, R., Lågstad, P., and Svolsbru, T.: Multiple
668 episodes of fluid flow in the SW Barents Sea (Loppa High) evidenced by gas flares, pockmarks and gas hydrate
669 accumulation, *Earth and Planetary Science Letters*, 331, 305-314, 2012.

670 Consolaro, C., Rasmussen, T., Panieri, G., Mienert, J., Bünz, S., and Szybor, K.: Carbon isotope ($\delta^{13}\text{C}$)
671 excursions suggest times of major methane release during the last 14 kyr in Fram Strait, the deep-water
672 gateway to the Arctic, *Climate of the Past*, 11, 669-685, 2015.

673 Crane, K., Sundvor, E., Buck, R., and Martinez, F.: Rifting in the northern Norwegian-Greenland Sea: Thermal
674 tests of asymmetric spreading, *Journal of Geophysical Research: Solid Earth*, 96, 14529-14550, 1991.

675 Crane, K., Doss, H., Vogt, P., Sundvor, E., Cherkashov, G., Poroshina, I., and Joseph, D.: The role of the
676 Spitsbergen shear zone in determining morphology, segmentation and evolution of the Knipovich Ridge, *Marine
677 geophysical researches*, 22, 153-205, 2001.

678 Crutchley, G. J., Berndt, C., Geiger, S., Klaeschen, D., Papenberg, C., Klauke, I., Hornbach, M. J., Bangs, N. L., and
679 Maier, C.: Drivers of focused fluid flow and methane seepage at south Hydrate Ridge, offshore Oregon, USA,
680 *Geology*, 41, 551-554, 2013.

681 Davies, R. J., Mathias, S. A., Moss, J., Hustoft, S., and Newport, L.: Hydraulic fractures: How far can they go?,
682 *Marine and petroleum geology*, 37, 1-6, 2012.

683 DeMets, C., Gordon, R. G., and Argus, D. F.: Geologically current plate motions, *Geophysical Journal
684 International*, 181, 1-80, 2010.

685 DeVore, J. R., and Sawyer, D. E.: Shear strength of siliciclastic sediments from passive and active margins (0–100
686 m below seafloor): insights into seismic strengthening, in: *Submarine Mass Movements and their
687 Consequences*, Springer, 173-180, 2016.

688 Dickens, G. R.: Down the rabbit hole: Toward appropriate discussion of methane release from gas hydrate
689 systems during the Paleocene-Eocene thermal maximum and other past hyperthermal events, *Climate of the
690 Past*, 7, 831-846, 2011.

691 Dumke, I., Burwicz, E. B., Berndt, C., Klaeschen, D., Feseker, T., Geissler, W. H., and Sarkar, S.: Gas hydrate
692 distribution and hydrocarbon maturation north of the Knipovich Ridge, western Svalbard margin, *Journal of*
693 *Geophysical Research: Solid Earth*, 121, 1405-1424, 2016.

694 Ehlers, B.-M., and Jokat, W.: Subsidence and crustal roughness of ultra-slow spreading ridges in the northern
695 North Atlantic and the Arctic Ocean, *Geophysical Journal International*, 177, 451-462, 2009.

696 Eiken, O., and Hinz, K.: Contourites in the Fram Strait, *Sedimentary Geology*, 82, 15-32, 1993.

697 Eldholm, O., Faleide, J. I., and Myhre, A. M.: Continent-ocean transition at the western Barents Sea/Svalbard
698 continental margin, *Geology*, 15, 1118-1122, 1987.

699 Engen, Ø., Faleide, J. I., and Dyreng, T. K.: Opening of the Fram Strait gateway: A review of plate tectonic
700 constraints, *Tectonophysics*, 450, 51-69, 2008.

701 Faleide, J., Gudlaugsson, S., Eldholm, O., Myhre, A., and Jackson, H.: Deep seismic transects across the sheared
702 western Barents Sea-Svalbard continental margin, *Tectonophysics*, 189, 73-89, 1991.

703 Faleide, J. I., Solheim, A., Fiedler, A., Hjelstuen, B. O., Andersen, E. S., and Vanneste, K.: Late Cenozoic evolution
704 of the western Barents Sea-Svalbard continental margin, *Global and Planetary Change*, 12, 53-74, 1996.

705 Faulkner, D., Jackson, C., Lunn, R., Schlische, R., Shipton, Z., Wibberley, C., and Withjack, M.: A review of recent
706 developments concerning the structure, mechanics and fluid flow properties of fault zones, *Journal of Structural*
707 *Geology*, 32, 1557-1575, 2010.

708 Fejerskov, M., and Lindholm, C.: Crustal stress in and around Norway: an evaluation of stress-generating
709 mechanisms, *Geological Society, London, Special Publications*, 167, 451-467, 2000.

710 Fertl, W.: Abnormal Formation Pressures: implications to exploration, drilling and production of oil and gas
711 reservoirs. *Development in Petroleum Science 2*. Elsevier Scientific Publications Company Amsterdam, 1976.

712 Fjeldskaar, W., and Amantov, A.: Effects of glaciations on sedimentary basins, *Journal of Geodynamics*, 118, 66-
713 81, 2018.

714 Franek, P., Plaza-Faverola, A., Mienert, J., Buenz, S., Ferré, B., and Hubbard, A.: Microseismicity linked to gas
715 migration and leakage on the Western Svalbard Shelf, *Geochemistry, Geophysics, Geosystems*, 18, 4623-4645,
716 2017.

717 Gaina, C., Nikishin, A., and Petrov, E.: Ultraslow spreading, ridge relocation and compressional events in the East
718 Arctic region: A link to the Eureka orogeny?, *arktos*, 1, 16, 2015.

719 Geersen, J., Scholz, F., Linke, P., Schmidt, M., Lange, D., Behrmann, J. H., Völker, D., and Hensen, C.: Fault zone
720 controlled seafloor methane seepage in the rupture area of the 2010 Maule Earthquake, Central Chile,
721 *Geochemistry, Geophysics, Geosystems*, 17, 4802-4813, 2016.

722 Grauls, D., and Baleix, J.: Role of overpressures and in situ stresses in fault-controlled hydrocarbon migration: A
723 case study, *Marine and Petroleum Geology*, 11, 734-742, 1994.

724 Grunnaleite, I., Fjeldskaar, W., Wilson, J., Faleide, J., and Zweigel, J.: Effect of local variations of vertical and
725 horizontal stresses on the Cenozoic structuring of the mid-Norwegian shelf, *Tectonophysics*, 470, 267-283,
726 2009.

727 Gölke, M., and Coblenz, D.: Origins of the European regional stress field, *Tectonophysics*, 266, 11-24, 1996.

728 Heidbach, O., Rajabi, M., Reiter, K., and Ziegler, M.: World stress map 2016, *Science*, 277, 1956-1962, 2016.

729 Hillis, R. R.: Coupled changes in pore pressure and stress in oil fields and sedimentary basins, *Petroleum*
730 *Geoscience*, 7, 419-425, 2001.

731 Hong, W. L., Sauer, S., Panieri, G., Ambrose, W. G., James, R. H., Plaza-Faverola, A., and Schneider, A.: Removal
732 of methane through hydrological, microbial, and geochemical processes in the shallow sediments of pockmarks
733 along eastern Vestnesa Ridge (Svalbard), *Limnology and Oceanography*, 61, 2016.

734 Hovland, M., and Sommerville, J. H.: Characteristics of two natural gas seepages in the North Sea, *Marine and*
735 *Petroleum Geology*, 2, 319-326, 1985.

736 Hovland, M.: On the self-sealing nature of marine seeps, *Continental Shelf Research*, 22, 2387-2394, 2002.

737 Hunter, S., Goldobin, D., Haywood, A., Ridgwell, A., and Rees, J.: Sensitivity of the global submarine hydrate
738 inventory to scenarios of future climate change, *Earth and Planetary Science Letters*, 367, 105-115, 2013.

739 Hustoft, S., Bünz, S., and Mienert, J.: Three-dimensional seismic analysis of the morphology and spatial
740 distribution of chimneys beneath the Nyegga pockmark field, offshore mid-Norway, *Basin Research*, 22, 465-
741 480, 2010.

742 Hustoft, S., Bunz, S., Mienert, J., Chand, S.: Gas hydrate reservoir and active methane-venting province in
743 sediments on < 20 Ma young oceanic crust in the Fram Strait, offshore NW-Svalbard, *Earth and Planetary*
744 *Science Letters*, 284, 12-24, 10.1016/j.epsl.2009.03.038, 2009.

745 Jakobsson, M., Backman, J., Rudels, B., Nycander, J., Frank, M., Mayer, L., Jokat, W., Sangiorgi, F., O'Regan, M.,
746 and Brinkhuis, H.: The early Miocene onset of a ventilated circulation regime in the Arctic Ocean, *Nature*, 447,
747 986-990, 2007.

748 Jansen, E., Sjøholm, J., Bleil, U., and Erichsen, J.: Neogene and Pleistocene glaciations in the northern
749 hemisphere and late Miocene—Pliocene global ice volume fluctuations: Evidence from the Norwegian Sea, in:
750 *Geological History of the Polar Oceans: Arctic versus Antarctic*, Springer, 677-705, 1990.

751 Jansen, E., and Sjøholm, J.: Reconstruction of glaciation over the past 6 Myr from ice-borne deposits in the
752 Norwegian Sea, *Nature*, 349, 600, 1991.

753 Johnson, J. E., Mienert, J., Plaza-Faverola, A., Vadakkepuliymbatta, S., Knies, J., Bünz, S., Andreassen, K., and
754 Ferré, B.: Abiotic methane from ultraslow-spreading ridges can charge Arctic gas hydrates, *Geology*, G36440.
755 36441, 2015.

756 Jokat, W., Lehmann, P., Damaske, D., and Nelson, J. B.: Magnetic signature of North-East Greenland, the Morris
757 Jesup Rise, the Yermak Plateau, the central Fram Strait: constraints for the rift/drift history between Greenland
758 and Svalbard since the Eocene, *Tectonophysics*, 691, 98-109, 2016.

759 Judd, A., and Hovland, M.: *Seabed fluid flow: the impact on geology, biology and the marine environment*,
760 Cambridge University Press, 2009.

761 Jung, N.-H., Han, W. S., Watson, Z., Graham, J. P., and Kim, K.-Y.: Fault-controlled CO₂ leakage from natural
762 reservoirs in the Colorado Plateau, East-Central Utah, *Earth and Planetary Science Letters*, 403, 358-367, 2014.

763 Karstens, J., and Berndt, C.: Seismic chimneys in the Southern Viking Graben—Implications for palaeo fluid
764 migration and overpressure evolution, *Earth and Planetary Science Letters*, 412, 88-100, 2015.

765 Karstens, J., Haflidason, H., Becker, L. W., Berndt, C., Rüpke, L., Planke, S., Liebetrau, V., Schmidt, M., and
766 Mienert, J.: Glacigenic sedimentation pulses triggered post-glacial gas hydrate dissociation, *Nature*
767 *communications*, 9, 635, 2018.

768 Keiding, M., Lund, B., and Árnadóttir, T.: Earthquakes, stress, and strain along an obliquely divergent plate
769 boundary: Reykjanes Peninsula, southwest Iceland, *Journal of Geophysical Research: Solid Earth*, 114, 2009.

770 Knies, J., Matthiessen, J., Vogt, C., Laberg, J. S., Hjelstuen, B. O., Smelror, M., Larsen, E., Andreassen, K., Eidvin,
771 T., and Vorren, T. O.: The Plio-Pleistocene glaciation of the Barents Sea–Svalbard region: a new model based on
772 revised chronostratigraphy, *Quaternary Science Reviews*, 28, 812-829,
773 <http://dx.doi.org/10.1016/j.quascirev.2008.12.002>, 2009.

774 Knies, J., Daszinnies, M., Plaza-Faverola, A., Chand, S., Sylta, Ø., Bünz, S., Johnson, J. E., Mattingsdal, R., and
775 Mienert, J.: Modelling persistent methane seepage offshore western Svalbard since early Pleistocene, *Marine*
776 *and Petroleum Geology*, 91, 800-811, 2018.

777 Lindholm, C. D., Bungum, H., Hicks, E., and Villagran, M.: Crustal stress and tectonics in Norwegian regions
778 determined from earthquake focal mechanisms, Geological Society, London, Special Publications, 167, 429-439,
779 2000.

780 Lund, B., and Townend, J.: Calculating horizontal stress orientations with full or partial knowledge of the
781 tectonic stress tensor, *Geophysical Journal International*, 170, 1328-1335, 2007.

782 Lund, B., Schmidt, P., and Hieronymus, C.: Stress evolution and fault stability during the Weichselian glacial
783 cycle, Swedish Nuclear Fuel and Waste Management Co, Stockholm, Sweden, Tech. Rep. TR-09-15, 2009.

784 Lund, B., and Schmidt, P.: Stress evolution and fault stability at Olkiluoto during the Weichselian glaciation,
785 Report for Posiva Oy, 2011.

786 Madrussani, G., Rossi, G., and Camerlenghi, A.: Gas hydrates, free gas distribution and fault pattern on the west
787 Svalbard continental margin, *Geophysical Journal International*, 180, 666-684, 2010.

788 Mattingdal, R., Knies, J., Andreassen, K., Fabian, K., Husum, K., Grøsfjeld, K., and De Schepper, S.: A new 6 Myr
789 stratigraphic framework for the Atlantic–Arctic Gateway, *Quaternary Science Reviews*, 92, 170-178, 2014.

790 Mau, S., Römer, M., Torres, M. E., Bussmann, I., Pape, T., Damm, E., Geprägs, P., Wintersteller, P., Hsu, C.-W.,
791 and Loher, M.: Widespread methane seepage along the continental margin off Svalbard—from Bjørnøya to
792 Kongsfjorden, *Scientific reports*, 7, 42997, 2017.

793 Minshull, T., and White, R.: Sediment compaction and fluid migration in the Makran accretionary prism, *Journal*
794 *of Geophysical Research: Solid Earth*, 94, 7387-7402, 1989.

795 Moore, J. C., and Vrolijk, P.: Fluids in accretionary prisms, *Reviews of Geophysics*, 30, 113-135, 1992.

796 Morgan, W. J.: 13. Hotspot tracks and the opening of the Atlantic and Indian Oceans, *The oceanic lithosphere*, 7,
797 443, 1981.

798 Myhre, A. M., and Eldholm, O.: The western Svalbard margin (74–80 N), *Marine and Petroleum Geology*, 5, 134-
799 156, 1988.

800 Naliboff, J., Lithgow-Bertelloni, C., Ruff, L., and de Koker, N.: The effects of lithospheric thickness and density
801 structure on Earth' s stress field, *Geophysical Journal International*, 188, 1-17, 2012.

802 Nasuti, A., and Olesen, O.: Chapter 4: Magnetic data. In: Hopper J.R., Funck T., Stoker T., Arting U., Peron-
803 Pinvidic G., Doornebal H. & Gaina C. (eds) *Tectonostratigraphic Atlas of the North-East Atlantic Region*.
804 Geological Survey of Denmark and Greenland (GEUS), Copenhagen, Denmark, 41–51. , 2014.

805 Okada, Y.: Surface deformation due to shear and tensile faults in a half-space, *Bulletin of the seismological*
806 *society of America*, 75, 1135-1154, 1985.

807 Olesen, O., Bungum, H., Dehls, J., Lindholm, C., Pascal, C., and Roberts, D.: Neotectonics, seismicity and
808 contemporary stress field in Norway—mechanisms and implications, *Quaternary Geology of Norway*, Geological
809 Survey of Norway Special Publication, 13, 145-174, 2013.

810 Panieri, G., Bünz, S., Fornari, D. J., Escartin, J., Serov, P., Jansson, P., Torres, M. E., Johnson, J. E., Hong, W., and
811 Sauer, S.: An integrated view of the methane system in the pockmarks at Vestnesa Ridge, 79° N, *Marine*
812 *Geology*, 390, 282-300, 2017.

813 Patton, H., Hubbard, A., Andreassen, K., Winsborrow, M., and Stroeven, A. P.: The build-up, configuration, and
814 dynamical sensitivity of the Eurasian ice-sheet complex to Late Weichselian climatic and oceanic forcing,
815 *Quaternary Science Reviews*, 153, 97-121, 2016.

816 Petersen, C. J., Bünz, S., Hustoft, S., Mienert, J., and Klaeschen, D.: High-resolution P-Cable 3D seismic imaging
817 of gas chimney structures in gas hydrated sediments of an Arctic sediment drift, *Marine and Petroleum*
818 *Geology*, doi: 10.1016/j.marpetgeo.2010.06.006, 1-14, DOI: 10.1016/j.marpetgeo.2010.06.006, 2010.

819 Planke, S., Eriksen, F. N., Berndt, C., Mienert, J., and Masson, D.: P-Cable high-resolution seismic, *Oceanography*,
820 22, 85, 2009.

821 Plaza-Faverola, A., Bünz, S., and Mienert, J.: Repeated fluid expulsion through sub-seabed chimneys offshore
822 Norway in response to glacial cycles, *Earth and Planetary Science Letters*, 305, 297-308,
823 10.1016/j.epsl.2011.03.001, 2011.

824 Plaza-Faverola, A., Bünz, S., Johnson, J. E., Chand, S., Knies, J., Mienert, J., and Franek, P.: Role of tectonic stress
825 in seepage evolution along the gas hydrate-charged Vestnesa Ridge, Fram Strait, *Geophys. Res. Lett.*, 42, 733-
826 742, 2015.

827 Plaza-Faverola, A., Henrys, S., Pecher, I., Wallace, L., and Klaeschen, D.: Splay fault branching from the Hikurangi
828 subduction shear zone: Implications for slow slip and fluid flow, *Geochemistry, Geophysics, Geosystems*, 17,
829 5009-5023, 2016.

830 Plaza-Faverola, A., Vadakkepuliambatta, S., Hong, W. L., Mienert, J., Bünz, S., Chand, S., and Greinert, J.:
831 Bottom-simulating reflector dynamics at Arctic thermogenic gas provinces: an example from Vestnesa Ridge,
832 offshore west-Svalbard, *Journal of Geophysical Research: Solid Earth*, 2017.

833 Portnov, A., Vadakkepuliambatta, S., Mienert, J., and Hubbard, A.: Ice-sheet-driven methane storage and
834 release in the Arctic, *Nature communications*, 7, 10314, 2016.

835 Riboulot, V., Thomas, Y., Berné, S., Jouet, G., and Cattaneo, A.: Control of Quaternary sea-level changes on gas
836 seeps, *Geophys. Res. Lett.*, 41, 4970-4977, 2014.

837 Riedel, M., Wallmann, K., Berndt, C., Pape, T., Freudenthal, T., Bergenthal, M., Bünz, S., and Bohrmann, G.: In
838 situ temperature measurements at the Svalbard Continental Margin: Implications for gas hydrate dynamics,
839 *Geochemistry, Geophysics, Geosystems*, 19, 1165-1177, 2018.

840 Roy, S., Senger, K., Braathen, A., Noormets, R., Hovland, M., and Olausson, S.: Fluid migration pathways to
841 seafloor seepage in inner Isfjorden and Adventfjorden, Svalbard, *Geological controls on fluid flow and seepage*
842 in western Svalbard fjords, Norway. An integrated marine acoustic study, 2014.

843 Salomatin, A., and Yusupov, V.: Acoustic investigations of gas “flares” in the Sea of Okhotsk, *Oceanology*, 51,
844 857, 2011.

845 Salomon, E., Koehn, D., Passchier, C., Hackspacher, P. C., and Glasmacher, U. A.: Contrasting stress fields on
846 correlating margins of the South Atlantic, *Gondwana research*, 28, 1152-1167, 2015.

847 Schiffer, C., Tegner, C., Schaeffer, A. J., Pease, V., and Nielsen, S. B.: High Arctic geopotential stress field and
848 implications for geodynamic evolution, *Geological Society, London, Special Publications*, 460, 441-465, 2018.

849 Schneider, A., Panieri, G., Lepland, A., Consolaro, C., Crémière, A., Forwick, M., Johnson, J., Plaza-Faverola, A.,
850 Sauer, S., and Knies, J.: Methane seepage at Vestnesa Ridge (NW Svalbard) since the Last Glacial Maximum,
851 *Quaternary Science Reviews*, 193, 98-117, 2018a.

852 Schneider, A., Panieri, G., Lepland, A., Consolaro, C., Crémière, A., Forwick, M., Johnson, J. E., Plaza-Faverola, A.,
853 Sauer, S., and Knies, J.: Methane seepage at Vestnesa Ridge (NW Svalbard) since the Last Glacial Maximum,
854 *Quaternary Science Reviews*, 193, 98-117, <https://doi.org/10.1016/j.quascirev.2018.06.006>, 2018b.

855 Sibson, R. H.: *Crustal stress, faulting and fluid flow*, Geological Society, London, Special Publications, 78, 69-84,
856 1994.

857 Skarke, A., Ruppel, C., Kodis, M., Brothers, D., and Lobecker, E.: Widespread methane leakage from the sea floor
858 on the northern US Atlantic margin, *Nature Geoscience*, 7, 657-661, 2014.

859 Smith, A. J., Mienert, J., Bünz, S., and Greinert, J.: Thermogenic methane injection via bubble transport into the
860 upper Arctic Ocean from the hydrate-charged Vestnesa Ridge, Svalbard, *Geochemistry, Geophysics,*
861 *Geosystems*, 2014.

862 Smith, S. B., Deniz Taylor: Deep-sea sediment compression curves: Some controlling factors, spurious
863 overconsolidation, predictions, and geophysical reproduction, *Marine Georesources and Geotechnology*, 17, 65-
864 81, 1999.

865 Somoza, L., León, R., Medialdea, T., Pérez, L. F., González, F. J., and Maldonado, A.: Seafloor mounds, craters
866 and depressions linked to seismic chimneys breaching fossilized diagenetic bottom simulating reflectors in the
867 central and southern Scotia Sea, Antarctica, *Global and Planetary Change*, 123, 359-373, 2014.

868 Steffen, H., Kaufmann, G., and Wu, P.: Three-dimensional finite-element modeling of the glacial isostatic
869 adjustment in Fennoscandia, *Earth and Planetary Science Letters*, 250, 358-375, 2006.

870 Stein, S., Cloetingh, S., Sleep, N. H., and Wortel, R.: Passive margin earthquakes, stresses and rheology, in:
871 *Earthquakes at North-Atlantic Passive Margins: Neotectonics and Postglacial Rebound*, Springer, 231-259, 1989.

872 Svensen, H., Planke, S., Malthe-Sørensen, A., Jamtveit, B., Myklebust, R., Eidem, T. R., and Rey, S. S.: Release of
873 methane from a volcanic basin as a mechanism for initial Eocene global warming, *Nature*, 429, 542-545, 2004.

874 Szybor, K., and Rasmussen, T. L.: Diagenetic disturbances of marine sedimentary records from
875 methane-influenced environments in the Fram Strait as indications of variation in seep intensity during the last
876 35 000 years, *Boreas*, 46, 212-228, 2017a.

877 Szybor, K., and Rasmussen, T. L.: Late glacial and deglacial palaeoceanographic changes at Vestnesa Ridge,
878 Fram Strait: Methane seep versus non-seep environments, *Palaeogeography, Palaeoclimatology, Palaeoecology*,
879 476, 77-89, 2017b.

880 Turcotte, D., Ahern, J., and Bird, J.: The state of stress at continental margins, *Tectonophysics*, 42, 1-28, 1977.

881 Turcotte, D. L., and Schubert, G.: *Geodynamics*, Cambridge University Press, New York, 2002.

882 Urlaub, M., Talling, P. J., Zervos, A., and Masson, D.: What causes large submarine landslides on low gradient (<
883 2°) continental slopes with slow (~ 0.15 m/kyr) sediment accumulation?, *Journal of Geophysical Research: Solid
884 Earth*, 120, 6722-6739, 2015.

885 Vanneste, M., Guidard, S., and Mienert, J.: Arctic gas hydrate provinces along the western Svalbard continental
886 margin, *Norwegian Petroleum Society Special Publications*, 12, 271-284, 2005.

887 Vis, G.-J.: *Geology and seepage in the NE Atlantic region*, Geological Society, London, Special Publications, 447,
888 SP447. 416, 2017.

889 Vogt, P. R., Crane, K., Sundvor, E., Max, M. D., and Pfirman, S. L.: Methane-generated (?) pockmarks on young,
890 thickly sedimented oceanic crust in the Arctic: Vestnesa ridge, Fram strait, *Geology*, 22, 255-258, 1994.

891 Waghorn, K. A., Bünz, S., Plaza-Faverola, A., and Johnson, J. E.: 3D Seismic Investigation of a Gas Hydrate and
892 Fluid Flow System on an Active Mid-Ocean Ridge; Svyatogor Ridge, Fram Strait, *Geochemistry, Geophysics,
893 Geosystems*, 2018.

894 Wallmann, K., Riedel, M., Hong, W., Patton, H., Hubbard, A., Pape, T., Hsu, C., Schmidt, C., Johnson, J., and
895 Torres, M.: Gas hydrate dissociation off Svalbard induced by isostatic rebound rather than global warming,
896 *Nature communications*, 9, 83, 2018.

897 Westbrook, G. K., Thatcher, K. E., Rohling, E. J., Piotrowski, A. M., Palike, H., Osborne, A. H., Nisbet, E. G.,
898 Minshull, T. A., Lanoiselle, M., James, R. H., Huhnerbach, V., Green, D., Fisher, R. E., Crocker, A. J., Chabert, A.,
899 Bolton, C., Beszczynska-Moller, A., Berndt, C., and Aquilina, A.: Escape of methane gas from the seabed along
900 the West Spitsbergen continental margin, *Geophys. Res. Lett.*, 36, 5, L1560810.1029/2009gl039191, 2009.

901 Zoback, M. D., and Zoback, M. L.: 34 State of stress in the Earth's lithosphere, *International Geophysics*, 81, 559-
902 XII, 2002.

903